SHP-1 dephosphorylates histone H2B to facilitate its ubiquitination during transcription

Prajakta Tathe[1,2] ID, K V S Rammohan Chowdary[1], Krushna Chandra Murmu[3] ID, Punit Prasad[3] ID & Subbareddy Maddika[1,*] ID

Abstract

Dynamic regulation of phosphorylation and dephosphorylation of histones is essential for eukaryotic transcription, but the enzymes engaged in histone dephosphorylation are not fully explored. Here, we show that the tyrosine phosphatase SHP-1 dephosphorylates histone H2B and plays a critical role during transition from the initiation to the elongation stage of transcription. Nuclear-localized SHP-1 is associated with the Paf1 complex at chromatin and dephosphorylates H2B at tyrosine 121. Moreover, knockout of SHP-1, or expression of a mutant mimicking constitutive phosphorylation of H2B Y121, leads to a reduction in genome-wide H2B ubiquitination, which subsequently causes defects in RNA polymerase II-dependent transcription. Mechanistically, we demonstrate that Y121 phosphorylation precludes H2B's interaction with the E2 enzyme, indicating that SHP-1-mediated dephosphorylation of this residue may be a prerequisite for efficient H2B ubiquitination. Functionally, we find that SHP-1-mediated H2B dephosphorylation contributes to maintaining basal autophagic flux in cells through the efficient transcription of autophagy and lysosomal genes. Collectively, our study reveals an important modification of histone H2B regulated by SHP-1 that has a role during eukaryotic transcription.

Introduction

Eukaryotic transcription is a highly complex and tightly coordinated process. Transcription cycle starts with an assembly of a preinitiation complex that promotes sequential recruitment of transcription factors and RNA Polymerase II (Pol II), followed by promoter melting, promoter escape leading to transcript elongation, and finally culminates with termination (Svejstrup, 2004). The formation of a preinitiation complex at the promoters does not always lead to productive transcription (Core et al, 2008). The occurrence of precise post-translational modifications on the C-terminal domain (CTD) of RNA Pol II and histone tails of the nucleosomes is vital to creating a dynamic environment for productive transcription (Li et al, 2007). Among many modifications of RNA Pol II CTD (Hsin & Manley, 2012), the role of ser5 and ser2 phosphorylation during transcription has been extensively characterized. CTD is phosphorylated at Ser5 residue by CDK7 to facilitate recruitment of enzymes for nascent mRNA capping and promote transition from preinitiation state to elongation (Ebmeier et al, 2017). Subsequently, Pol II gets phosphorylated at Ser2 by CDK9 (Marshall et al, 1996) and recently characterized CDK12 (Bartkowiak et al, 2010), during elongation step of the transcription. These two CTD modifications are dynamically regulated during transcription cycle, where phosphatases such as Scp1, Fcp1, SSU72, CDC14, Rtr1, Glc7 dephosphorylate Ser5 and Ser2 after Pol II entry to elongation state and at the end of transcription respectively to initiate a new cycle of transcription (Yeo et al, 2003; Fuda et al, 2012).

In addition to Pol II CTD modifications, histone modifications such as ubiquitination, acetylation, and methylation occur cotranscriptionally and play an essential role in productive transcription (Gates et al, 2017). Different histone marks recruit specific readers necessary for each step of the transcription cycle (e.g., H3K4me3/ TFIID for initiation, H3K9ac/SEC for pause release, H3K36me3/ DNMT3a/b for elongation, and H3K9me2/HP1γ for termination). High levels of H3K4me3 and multiple acetylated H3 and H4 lysine residues were found to be enriched at active promoters, whereas gene bodies of transcribed genes are enriched with H2BK120ub, H3K36me3, H3K79me2, and H3K79me3 (Chen et al, 2018). Additionally, dynamic phosphorylation of histones has been shown to play a vital role in coordinating transcription. For instance, phosphorylation of histone H3 at serine 10 and 28, and histone H2A on T120, is involved in the regulation of chromatin structure and function during transcription (Rossetto et al, 2012; Kim et al, 2013). Recent studies also highlight the importance of histone tyrosine phosphorylation during transcription regulation. For example, H2B Y37 phosphorylation was shown to attenuate the transcription of histone cluster genes and, on the other hand, H3 Y41 phosphorylation by JAK2 leads to

1 Laboratory of Cell Death and Cell Survival, Centre for DNA Fingerprinting and Diagnostics (CDFD), Hyderabad, India
2 Graduate Studies, Manipal Academy of Higher Education, Manipal, India
3 Epigenetic and Chromatin Biology Unit, Institute of Life Sciences, Bhubaneswar, India
*Corresponding author. Tel: +91 40 2721 6168. E-mail: msreddy@cdfd.org.in

transcriptional activation by preventing binding of HPIα to chromatin (Dawson *et al*, 2009; Mahajan *et al*, 2012). Interestingly, so far, all the emphasis has been given to kinases that modify histones, but little is known about the phosphatases responsible for histone dephosphorylation during transcription. Here, we report a tyrosine phosphatase SHP-1 as an important enzyme that reverses phosphorylation of Y121 residue on H2B, a new modification that plays an essential switching role during transcription.

SHP-1, a non-receptor tyrosine phosphatase encoded by the PTPN6 gene, is highly expressed in hematopoietic cells and moderately in several non-hematopoietic cell types (Craggs & Kellie, 2001). SHP-1 functions in multiple signaling pathways (growth factor and cytokine-dependent) in hematopoietic cells by controlling phosphorylation of varied substrates such as ZAP70, Syk, Crk II, Jak1, GSK3β, thus regulating a variety of cellular processes including cell proliferation, growth, and differentiation (Brockdorff *et al*, 1999; Dustin *et al*, 1999; Jiang *et al*, 2016; Azoulay-Alfaguter *et al*, 2017). Homozygous mutation in PTPN6 gene (PTPN6[me/me]) shows moth-eaten phenotype in mice. These mice develop chronic inflammation of the skin, autoimmunity, and eventually succumb to fatal pneumonitis (Van Zant & Shultz, 1989). By virtue of its antagonist function to the growth-promoting tyrosine kinase signaling in hematopoietic cells, SHP-1 has been suggested to be a candidate tumor suppressor gene in lymphoma and leukemias (Zhang *et al*, 2000). In contrast, SHP-1 protein is over-expressed in some non-lymphocytic cell lines, such as prostate cancer, breast and ovarian cancers, possibly suggesting that SHP-1 can play context-dependent negative or positive roles in regulating signal transduction pathway (Varone *et al*, 2020).

Results

SHP-1 interacts with chromatin-associated proteins

SHP-1 is known to be a predominantly cytoplasmic phosphatase in cells of hematopoietic origin; however, by virtue of a nuclear localization signal on its C-terminus, it has the potential to localize to the nucleus (Yang *et al*, 2002). We screened a panel of cells from hematopoietic and non-hematopoietic origin to understand the localization of SHP-1. While SHP-1 is majorly found in the cytoplasm of different hematopoietic cells (THP-1, Jurkat and U937), interestingly, it shows distinct nuclear localization in epithelial cells of non-hematopoietic origin derived from different human cancer tissues (breast epithelial line: MCF-7, colon epithelial cells: HCT116, Lung epithelial cell line: A549, embryonic kidney cells: 293T and cervical epithelial cells: HeLa) (Fig 1A). Similar nuclear localization of SHP-1 was also seen in epithelial cells of non-cancerous origin (Retinal pigment epithelial cells: RPE1, human mammary epithelial cells: MCF10A) (Fig EV1A). To test if the nuclear localization signal is specific for SHP-1, we generated an SHP-1 knockout line in MCF-7 breast epithelial cells using CRISPR (Fig EV1B). Wild-type MCF-7 cells display predominant SHP-1 nuclear localization, but the signal is completely lost in SHP-1 knockout cells (Fig EV1C). In addition, no SHP-1 signal was detected in MDA-MB-231 cell line (Fig EV1D), a breast cancer epithelial line that loses SHP-1 expression due to promoter hypermethylation (Yip *et al*, 2000), suggesting that the nuclear localization is specific for SHP-1. Furthermore, we observed

that SHP-1 displays a distinct punctate-like localization in the nucleus, prompting us to hypothesize that SHP-1 might be localizing to chromatin. Indeed, our biochemical fractionation experiments confirmed SHP-1 association with chromatin in different epithelial cells (Fig EV1E and F). Although SHP-1 was predominantly seen in the cytoplasm of different hematopoietic cells during our immunofluorescence studies, cell fractionation experiments revealed significant enrichment of SHP-1 at chromatin (Fig EV1G). Together, these data indicate that SHP-1 displays chromatin localization in a broad range of cells derived from hematopoietic as well as non-hematopoietic origin.

To investigate the role of chromatin-associated nuclear SHP-1 in cells, we analyzed the list of SHP-1-associated proteins derived through an interaction proteomics approach in our earlier study (Kumar *et al*, 2017). Tandem affinity purification with streptavidin-agarose beads and S-protein-agarose beads using lysates derived from cells expressing a triple-tagged SFB-SHP-1 followed by mass spectrometry analysis allowed us to discover several chromatin proteins associated with SHP-1. Among these proteins, we consistently found the components of Paf1 complex along with histone H2B in SHP-1 purified complex (Fig 1B). Paf1 complex (Paf1C) is a conserved multi-subunit complex (with Paf1, Ctr9, Cdc73, Rtf1, hSki8, and Leo1 as integral components) that plays a very critical role in various stages of RNA Polymerase II-dependent transcription cycle (Van Oss *et al*, 2017). Several studies have clearly established that Paf1C regulates transcription elongation as well as transcription termination via promoting different co-transcriptional histone modifications such as H2B ubiquitination (Van Oss *et al*, 2017). By using exogenously expressed proteins, we confirmed the interaction of Paf1 complex components specifically with SHP-1 (Fig 1C). Also, we confirmed the interaction of overexpressed myc-tagged histone H2B specifically with SHP-1 in cells (Fig 1D). Furthermore, we validated the interaction of endogenous SHP-1 with endogenous Paf1 complex proteins (Fig 1E) as well as histone H2B (Fig 1F) in cells by performing immunoprecipitation with SHP-1 specific antibody. Interaction of SHP-1 is with chromatin-bound H2B and not free histone, as other histones such as H2A, H3, and H4 were readily found in the immunoprecipitated complexes of SHP-1 (Fig EV1H). Bacterially purified recombinant GST-tagged H2B and MBP-tagged SHP-1 proteins interacted with each other, suggesting a direct interaction between SHP-1 and histone H2B (Fig 1G). Together, these data indicate that SHP-1, a well-known cytoplasmic phosphatase, localizes to nucleus where it is associated with new complexes at chromatin such as Paf1 complex and histones.

Nuclear SHP-1 is necessary for H2B ubiquitination

Paf1 complex is essential for histone H2B ubiquitination (Chen *et al*, 2021), but how exactly it promotes H2B ubiquitination in cells is not completely understood. Since we found that SHP-1 is associated with both Paf1 complex as well as histone H2B, we hypothesized that SHP-1 by associating with Paf1 complex might contribute to H2B ubiquitination. To test this hypothesis, we generated CRISPR-based SHP-1 knockout lines in 293T cells. While H2B ubiquitination is readily detected in wild-type 293T cells, SHP-1 knockout cells display severely diminished histone ubiquitination (Fig 2A and Appendix Fig S1A). Furthermore, to understand if nuclear-localized SHP-1 is necessary for mediating histone ubiquitination,
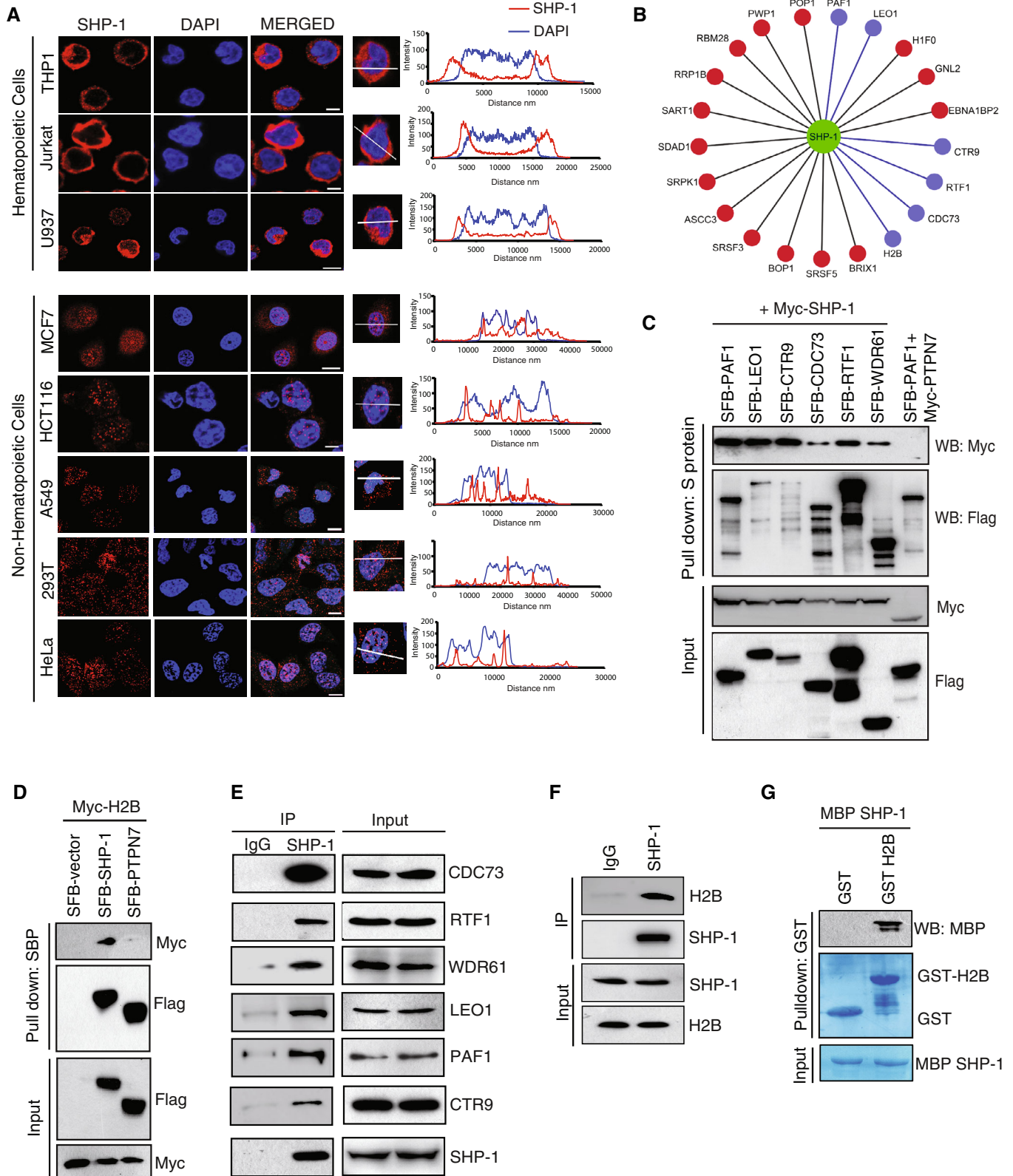
Figure 1.

Figure 1. Nuclear localized SHP-1 is associated with Paf complex and Histone H2B.

A Localization of endogenous SHP-1 in hematopoietic and non-hematopoietic cells was determined by confocal imaging after staining with SHP-1 antibody. DAPI was used for nuclear staining, Scale bar: 5 μm. Fluorescence intensities along the line drawn in a representative cell were obtained using Zen software and the co-localization plots were made using GraphPad (Red: SHP-1, Blue: DAPI).

B Network of nuclear proteins associated with SHP-1 is shown. SFB-GFP purification was used as control to filter out non-specific interactions. The list of SFB-SHP-1 and SFB-GFP-associated proteins was derived from our earlier study (Kumar *et al*, 2017). Paf complex components and Histone H2B are highlighted in blue in the network.

C SFB tagged PAF1, SFB-LEO1, SFB-CTR9, SFB-CDC73, SFB-RTF1, SFB-WDR61 along with Myc SHP-1 or Myc PTPN7 were transfected in 293T cells and interaction of SHP-1 with PAF complex components was detected by immunoblotting with Myc antibody after S protein beads pulldown in the presence of TurboNuclease.

D SFB empty vector, SFB SHP-1, or SFB PTPN7 was co-transfected with Myc tagged H2B in 293T cells. The interaction of H2B with SHP-1 was detected through immunoblotting using Myc antibody after pulldown with streptavidin sepharose beads.

E Endogenous association of SHP-1 with Paf1 complex subunits (CDC73, RTF1, WDR61, LEO1, Paf1, CTR9) was detected by immunoblotting after performing immuno-precipitation with either IgG or SHP-1 antibody.

F Immunoprecipitation (IP) with control IgG or anti-SHP-1 antibody was performed with extracts prepared from MCF7 cells and endogenous association of H2B with SHP-1 was detected by immunoblotting.

G Glutathione Sepharose beads immobilized with bacterially expressed recombinant GST or GST-H2B proteins were incubated with bacterially purified recombinant MBP-SHP-1. The association of SHP-1 with H2B was detected by immunoblotting with MBP antibody. Expression of GST, GST-H2B, and MBP SHP-1 was shown by Coomassie staining.

Source data are available online for this figure.

we generated an SHP-1 NLS mutant that is defective in nuclear localization (Fig EV2A) and unable to interact with histone H2B (Fig EV2B). Expression of constitutively active SHP-1 (ΔSH2) with intact NLS, but not NLS mutant, rescues H2B ubiquitination that was lost in SHP-1 knockout cells, suggesting that nuclear localization of SHP-1 is required for histone ubiquitination (Fig 2B and Appendix Fig S1B). SHP-1 being a phosphatase, we next tested if its catalytic activity in the nucleus is required for promoting H2B ubiquitination. Expression of wild-type, but not catalytically inactive mutant of SHP1 (C453S), could enhance H2B ubiquitination in SHP-1 knockout cells (Fig 2C and Appendix Fig S1C), thus suggesting the requirement of phosphatase activity in the nucleus to mediate H2B ubiquitination. Given that SHP-1 is a tyrosine phosphatase and its activity is required for H2B ubiquitination, we next tested if mutation of any tyrosine residue on H2B would alter its ubiquitination. H2B has 5 tyrosine residues and conversion of any of the tyrosines to phenyl alanine has no impact on its ubiquitination. However, mutation of Y121 residue to aspartic acid (a phospho-mimetic variant) completely abolished H2B ubiquitination (Figs 2D and EV2C), similar to that of H2B K120R (ubiquitination site) mutant. Mutation of Y121 to aspartic acid neither affected H2B presence in the nucleosome fraction (Fig EV2D) nor its ability to interact with other histones such as H2A, H3, and H4 (Fig EV2E), thus suggesting that the loss of ubiquitination in Y121D mutant is a direct effect of Y121 modification. Interestingly, Y121 is located adjacent to the site of H2B ubiquitination and our data suggest that the presence of a negative charge on this residue might negatively hamper the ubiquitination of K120 residue. To further test if this is indeed true, we performed *in vitro* ubiquitination assays using various bacterially purified recombinant H2B proteins. While wild-type H2B could be readily ubiquitinated *in vitro*, no ubiquitination was detected with Y121D mutant (Fig 2E). Loss of ubiquitination in Y121D mutant *in vitro* is not restricted to free histone as H2B Y121D mutant in H2A-H2B dimer also shows a similar defect in ubiquitination (Fig EV2F and Appendix Fig S1D). Furthermore, *in vitro* ubiquitination assays using synthesized histone peptides revealed that a non-phosphopeptide could be ubiquitinated efficiently, whereas phosphopeptide (pY121) fails to accept ubiquitin on K120 residue (Fig 2F). Therefore, these data suggest that a phosphate group on Y121 residue hampers H2B K120 ubiquitination and the nuclear-

localized SHP-1 might assist in H2B ubiquitination by removing the phosphate on H2B.

SHP-1 dephosphorylates histone H2B at Y121 residue

Since SHP-1 phosphatase activity is required for promoting H2B ubiquitination, we next sought to identify if histone H2B or any of the components of Paf1 complex are novel SHP-1 substrates in the nucleus. Previously, CDC73, one of the components of Paf1 complex, was shown to be dephosphorylated by SHP-2, a closely related phosphatase to SHP-1(Takahashi *et al*, 2011). In line with the earlier study, we observed that SHP-2 could readily dephosphorylate CDC73 *in vitro*; however, SHP-1 could not dephosphorylate CDC73 (Fig EV3A). We next tested if any of the other components of Paf1 complex are substrates of SHP-1. All the components of Paf1 complex purified individually from bacteria (Fig EV3B) were *in vitro* phosphorylated using 293T lysate and used as substrates for phosphatase assay. *In vitro* phosphatase assay using active SHP-1 (ΔSH2) (Fig EV3C) revealed that none of the Paf1 components were dephosphorylated by SHP-1 (Fig EV3D). Lack of phosphate release in the *in vitro* malachite green assay also confirmed that none of the Paf1 components are bona fide substrates of SHP-1 (Fig EV3E). Next, we tested if H2B is a new substrate of SHP-1. Tyrosine kinase SYK was shown to have the ability to transfer phosphate groups on various tyrosine residues on H2B (Sakai *et al*, 1991). Bacterially purified recombinant H2B was phosphorylated *in vitro* by using SYK and we utilized this phosphorylated H2B as a substrate in our phosphatase assays. We found that bacterially purified active SHP-1 readily releases phosphatase from H2B (Fig 3A). While active SHP-1 could dephosphorylate tyrosine residues, phosphatase inactive C/S mutant could not do so under *in vitro* conditions (Fig 3B and Appendix Fig S1E). Furthermore, *in vitro* phosphatase assay using the custom synthetic peptide containing phosphorylated residue at Y121 site confirmed that SHP-1 releases phosphate from H2B Y121 residue (Fig 3C). Tyrosine phosphorylation of H2B is also readily observed in cells, and deletion of SHP-1 in cells enhanced tyrosine phosphorylation (Fig EV4A and Appendix Fig S1F). Furthermore, while tyrosine phosphorylation on wild-type H2B is readily detected in cells, phosphorylation is severely hampered in Y121F mutant, clearly suggesting that Y121 residue is a bona fide tyrosine
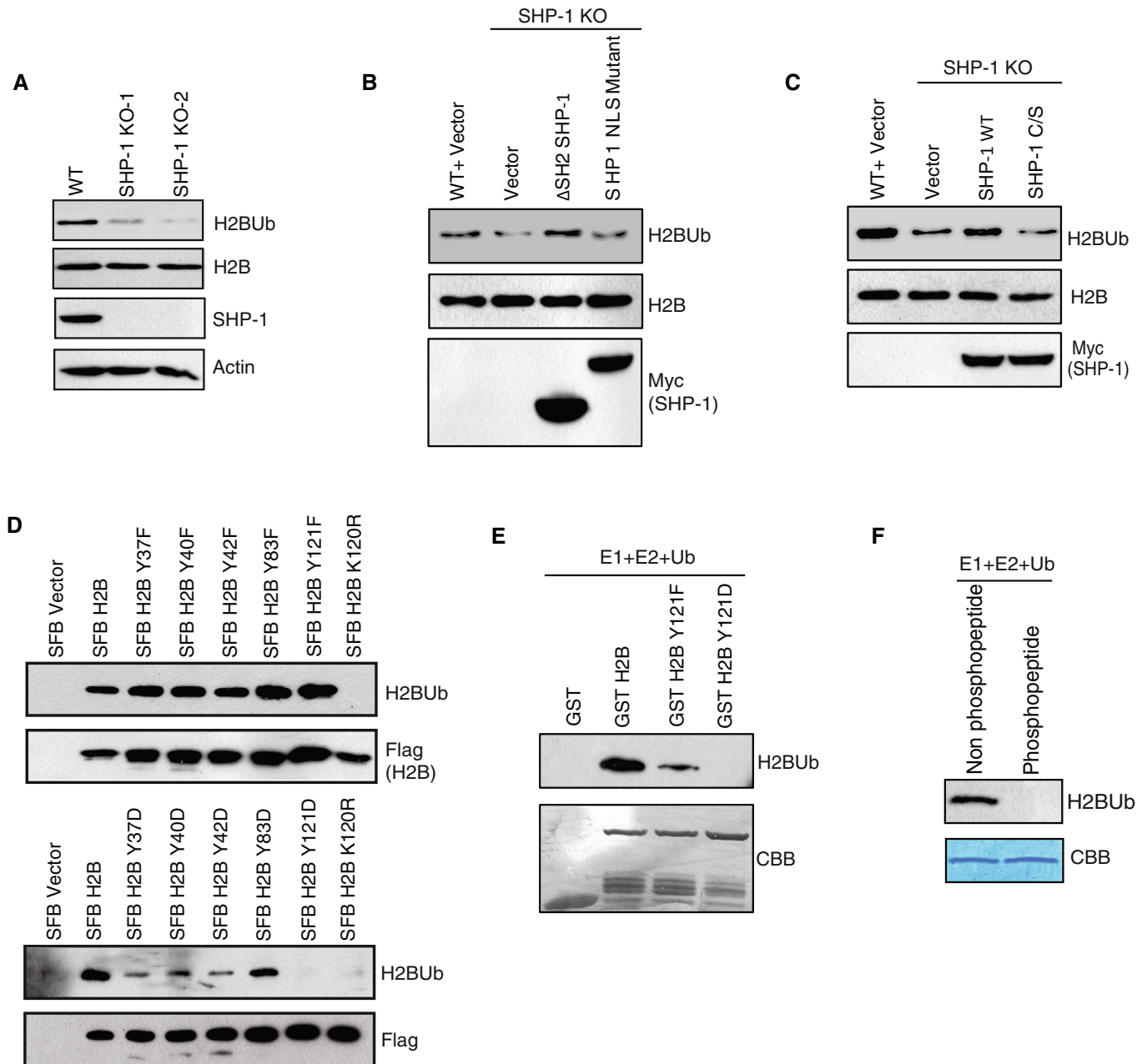
Figure 2. SHP-1 is required for efficient H2B ubiquitination.

A   Nuclear extracts of WT and SHP-1 knockout cells (derived from two independent guide RNAs) were made and the levels of H2BUb were detected.

B   Wild-type (WT) 293T cells along with SHP-1 KO cells transfected with either Myc vector, Myc SHP-1 ΔSH2, or Myc SHP-1 NLS mutant were lysed. H2BUb levels were determined using specific antibody.

C   WT and SHP-1 KO 293T cells transfected with Myc vector, Myc SHP-1, or Myc SHP-1 C/S (C453S) mutant were lysed. H2BUb levels were determined using specific antibody.

D   H2B WT along with the indicated Y/F and Y/D mutants were transfected into 293T cells. Histone extract was prepared from cells transfected with each construct and subjected to Western blotting with anti-H2B and anti-H2BUb antibodies.

E   *In vitro* ubiquitination assay was performed using bacterially purified GST, GST-tagged H2B, and its mutants as substrates. Recombinant E1, E2(UBE2A), and ubiquitin were included in each reaction. Ubiquitination was detected by H2BUb antibody.

F   *In vitro* ubiquitination was performed using biotin-tagged non-phospho and phospho (pY121) peptide of H2B as substrates in the presence of E1 and E2. H2BUb was detected by immunoblotting with specific antibody.

Source data are available online for this figure.

phosphorylation site in cells (Fig EV4B and Appendix Fig S1G). To further understand if SHP-1 dephosphorylates H2B at Y121 residue, we generated a polyclonal Y121 phospho-specific antibody. We validated the antibody *in vitro* using phospho-specific Y121 synthetic peptide (Fig EV4C) and in cells using an Y121F mutant (Fig EV4D

and Appendix Fig S1H). We found that the newly generated antibody specifically detects H2B phosphorylated at Y121 residue. Phospho-Y121 signal was lost upon treatment of H2B with λ-phosphatase (Fig EV4E and Appendix Fig S1I). In addition, preincubation of antibody with phosphospecific Y121 synthetic peptide,
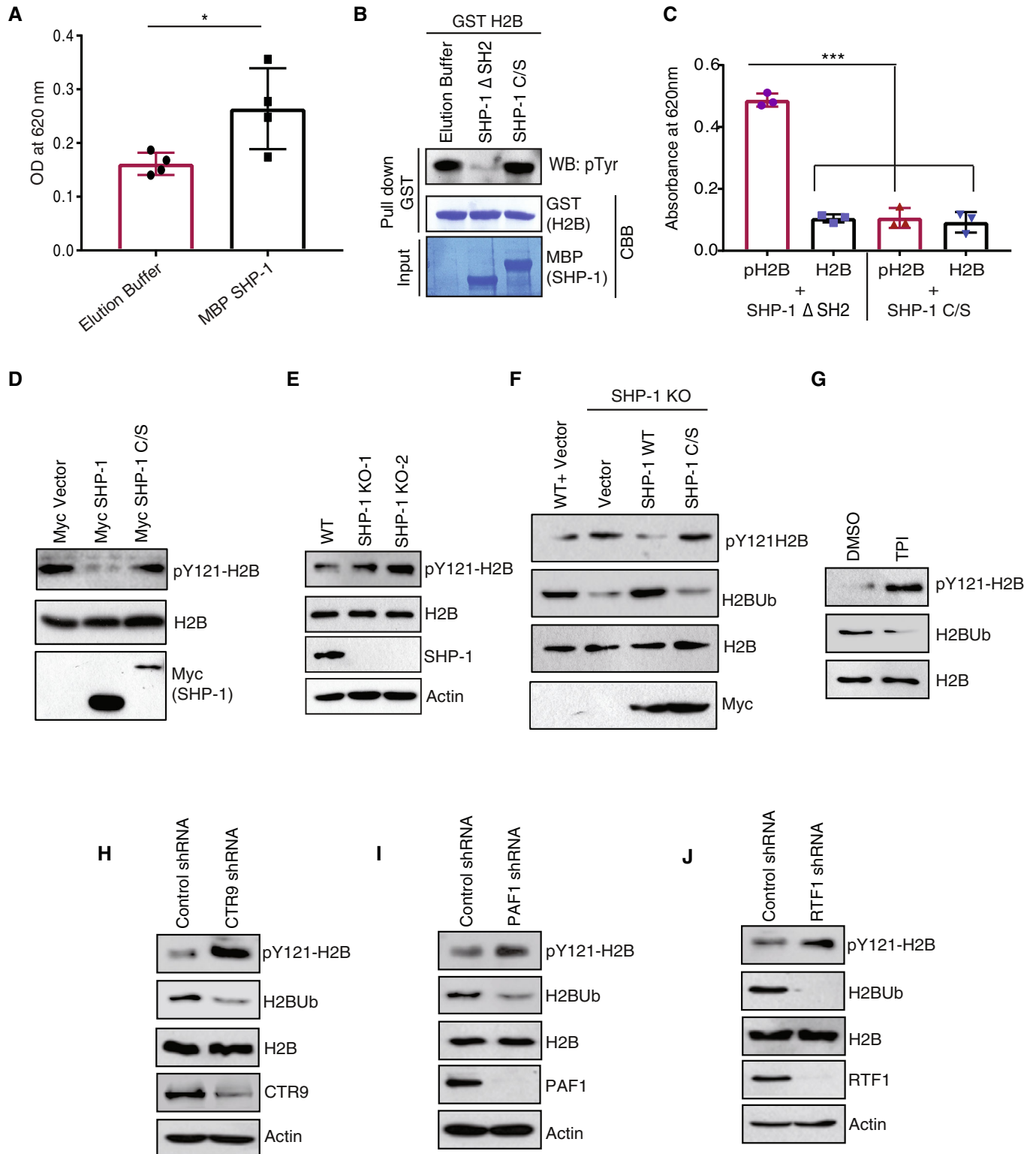

Figure 3.

Figure 3. Histone H2B is a new substrate for SHP-1.

A   *In vitro* phosphorylated GST H2B by Syk kinase was incubated with bacterially purified recombinant wild-type SHP-1 or elution buffer and the amount of released phosphate was assayed colorimetrically using the malachite green reagent (A620 nm). Data represent mean absorbance from four independent experiments. Error bar indicates SD; *P < 0.05, by Student's *t* test.

B   Bacterially purified GST H2B was subjected to *in vitro* kinase assay using HEK293T-cell lysate, and then phosphorylated proteins were incubated with either bacterially purified MBP tagged constitutively active (SHP-1 ΔSH2), or catalytically inactive SHP-1 C/S mutant. The phosphorylation status of recombinant H2B was detected by immunoblotting with phospho-tyrosine antibody.

C   Phospho (pH2B) Y121 and non-phospho peptide of H2B was incubated with constitutively active (SHP-1 ΔSH2) or catalytically inactive mutant (C/S) of SHP-1 and the released phosphate was assayed colorimetrically using the malachite green reagent (A620 nm). *n* = 3 independent experiments, Error bars indicate SD; ***P < 0.001 (one-way ANOVA, Tukey's multiple comparison test).

D   293T cells were transfected with vector, Myc tagged SHP-1 WT or C/S mutant. The phosphorylation status of endogenous H2B was detected by immunoblotting with pY121-H2B antibody.

E   Nuclear extracts of 293T WT and SHP-1 KO cells were made and the levels of H2B phosphorylation were detected using pY121-H2B antibody.

F   Wild-type (WT) along with SHP-1 KO 293T cells transfected with either Myc vector, Myc SHP-1 or Myc SHP-1 C/S mutants were lysed. Levels of pY121-H2B and H2BUb were determined using specific antibodies.

G   293T Cells were treated with SHP-1 inhibitor TPI (50 nM) for 1 h and levels of pY121-H2B were determined using pY121H2B antibody.

H–J   MCF7 cells were transduced with (H) CTR9 shRNA, (I) Paf1 shRNA, or (J) RTF1 shRNA along with control shRNA. Post 72 h, cells were collected and lysed to isolate soluble and nuclear fractions. Levels of phosphorylated and ubiquitinated H2B were detected by immunoblotting with indicated specific antibodies.

Source data are available online for this figure.

but not non-phospho peptide, failed to detect a phospho-signal on H2B in wild-type and SHP-1 KO cells, thus indicating that the newly generated antibody specifically detects phosphorylated H2B (Fig EV4F). Furthermore, the antibody detects phosphorylation on histone H2B, but not on any other histones (Fig EV4G), thus confirming the specificity of the antibody. By using a phospho-specific antibody, we found that phosphorylation at H2B Y121 residue is reduced in cells expressing wild-type SHP-1, but not catalytically inactive C/S mutant (Fig 3D and Appendix Fig S2A). Similar data were obtained under *in vitro* conditions, where active SHP-1, but not the catalytically inactive mutant, dephosphorylates H2B at Y121 residue (Fig EV4H and Appendix Fig S2B). On the other hand, deletion of SHP-1 in cells enhanced phosphorylation of Y121 residue (Fig 3E and Appendix Fig S2C). The enhanced phosphorylation in knockout cells is due to specific deletion of SHP-1 since re-expression of wild-type SHP-1, but not inactive C/S mutant, reduced pY121 levels in SHP-1 knockout cells (Fig 3F and Appendix Fig S2D). In addition, we demonstrated that pharmacological inhibition of SHP-1 by treating cells with a specific inhibitor TPI enhanced pY121 levels (Fig 3G and Appendix Fig S2E), followed by reduced H2B ubiquitination in cells. Together, these data clearly suggest that histone H2B is a novel substrate of SHP-1 in cells and the dephosphorylation occurs specifically at Y121 residue on H2B. Furthermore, as SHP-1 is associated with H2B along with Paf1 complex, we next tested if Paf complex participates in SHP-1 mediated H2B dephosphorylation. Depletion of CTR9 (Fig 3H), Paf1 (Fig 3I), or RTF1 (Fig 3J) (Appendix Fig S2F–H) using individual shRNAs significantly enhanced the phosphorylation levels of H2B Y121 in cells. Thus, these data indicate that Paf1 complex-associated SHP-1 removes phosphate group from H2B Y121 residue and thereby promotes efficient H2B K120 ubiquitination.

H2B Y121 dephosphorylation is required for E2 binding

We next sought to understand the molecular mechanism on how phosphorylation at Y121 residue prevents H2B ubiquitination in cells. H2B ubiquitination in cells is carried out by concerted action of E2 (Ube2A in humans or Rad6 in yeast) and E3 (RNF20/40 in humans or BRE1 in yeast) enzymes. Firstly, we tested if H2B Y121 phosphorylation modulates the binding of E3 enzymes. No

detectable changes were observed in binding of RNF20 with Y121F and Y121D mutants in comparison with wild-type H2B (Fig 4A), thereby suggesting that Y121 phosphorylation has no effect on E3 ligase binding with H2B. Next, we tested if Y121 phosphorylation modulates E2 binding with the substrate. While Y121F mutant binds with Ube2A as efficiently as wild-type H2B, mutation of Y121D that mimics phosphorylation led to severe loss of interaction between H2B and Ube2A in cells (Fig 4B and Appendix Fig S3A and B). On the other hand, we also confirmed the loss of interaction between H2B Y121D mutant and Ube2A under *in vitro* conditions using bacterially purified recombinant proteins (Fig 4C and Appendix Fig S3C). Furthermore, we tested if indeed addition of phosphate group on H2B impedes its binding to Ube2A. While Ube2A efficiently interacts with unphosphorylated H2B, phosphorylation of H2B at Y121 residue *in vitro* hampered its interaction with Ube2A (Fig 4D and Appendix Fig S3D), thus clearly suggesting that phosphorylation of H2B at Y121 residue prevents its association of E2 enzyme. As we have demonstrated that SHP-1 dephosphorylates H2B at Y121 residue, we next tested if SHP1 activity is necessary for H2B binding with E2 enzyme. While no detectable changes in total protein levels of either E3 or E2 enzymes were seen (Appendix Fig S3E), interaction of H2B with Ube2A is severely hampered in SHP-1 knock out cells in comparison to wild-type cells (Fig 4E and Appendix Fig S3F). Furthermore, pharmacological inactivation of SHP-1 activity by treating cells with a specific inhibitor TPI also caused loss of H2B interaction with Ube2A (Fig 4F and Appendix Fig S3G). Together, these results suggest that H2B phosphorylation at Y121 residue precludes its interaction with E2 enzyme and therefore SHP-1-mediated dephosphorylation of this residue is necessary for providing substrate access to E2 enzyme that leads to H2B ubiquitination. Thus, loss of SHP1 protein or its activity leads to loss of H2B ubiquitination due to inability of H2B to interact with E2 enzymatic machinery.

SHP-1 localizes to sites of transcription and facilitates cellular transcription

H2B K120 ubiquitination is critical for cellular transcription. As we have shown that SHP-1 is necessary for efficient H2B ubiquitination in cells, we next tested if SHP-1 localizes to sites of active
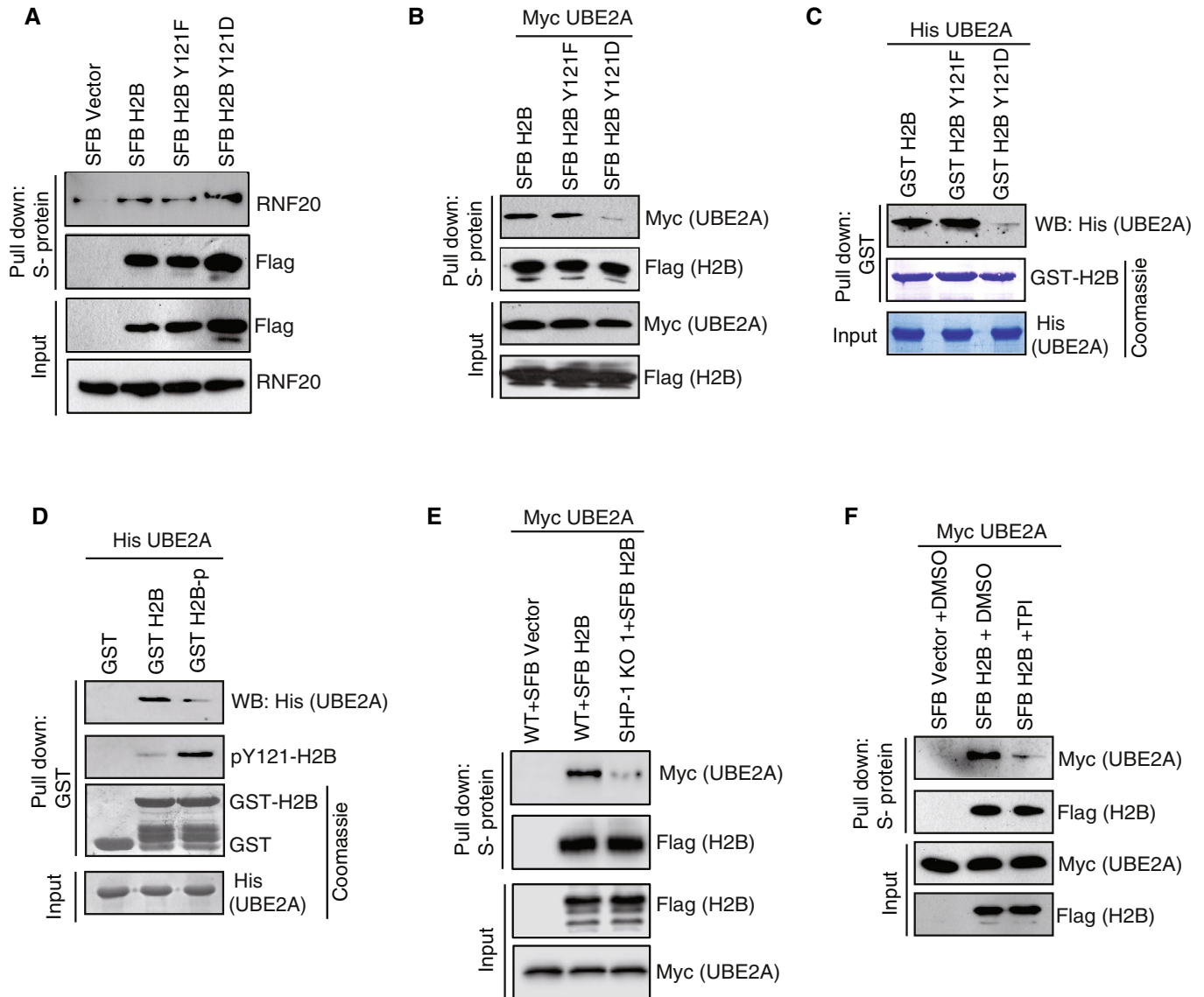
Figure 4. H2B Y121 dephosphorylation by SHP-1 is necessary for E2 binding.

A Cell lysates derived from 293T cells transfected with empty vector, SFB-tagged H2B, H2B Y121F, or H2B Y121D constructs were pulled down with S-protein agarose beads. RNF20 interaction with H2B was detected by immunoblotting with specific antibody.

B HEK293T cells were co-transfected with the SFB-tagged H2B, H2B Y121F, or H2B Y121D constructs along with Myc-tagged UBE2A. Cell lysates were pulled down with S-protein beads, and interaction was detected by immunoblotting with Myc antibody.

C Glutathione Sepharose beads bound with bacterially expressed recombinant GST-H2B, GST H2B Y121F and GST-H2B Y121D proteins were incubated with bacterially purified recombinant His UBE2A, and interaction of UBE2A with H2B was detected by immunoblotting with His antibody. Recombinant protein expression and pull-down were shown by Coomassie staining.

D Bacterially purified GST, GST H2B, and GST H2B-p (phosphorylated using Syk) were incubated with recombinant His UBE2A, and interaction of UBE2A with H2B was detected by immunoblotting with His antibody. Recombinant protein expression and pulldown were shown by Coomassie staining.

E WT 293T cells along with SHP-1 KO were co-transfected with SFB vector or SFB H2B along with Myc UbE2A. Cell lysates were pulldown using S-protein beads, and interaction of UBE2A with H2B was determined by Western blotting with the indicated antibodies.

F HEK293T cells were transfected with SFB vector or SFB H2B along with Myc UBE2A. Cells were treated with SHP-1 inhibitor TPI (50 nM) for 1 h after 24 h of transfection. Cell lysates were subjected to pulldown with S-protein beads, and Western blotting was performed using specific antibodies.

Source data are available online for this figure.

transcription on chromatin. In order to determine if SHP-1 co-localizes to transcription machineries in cells, we performed immunofluorescence staining with specific antibodies against CDK9, RNA Pol II, RNA Pol II Ser5P, and RNA Pol II Ser2P. Our super-resolution imaging analysis has revealed that SHP-1 readily localizes to CDK9 along with RNA Pol II, RNA Pol II Ser5P, and RNA Pol II Ser2P (Fig 5A). Several studies have clearly shown that CDK9 and RNA Pol II Ser5P mostly occupy the promoter/transcription start site

of genes and that RNA Pol II Ser2P is enriched over the gene body and is associated with transcriptional elongation (Komarnitsky *et al*, 2000). Although SHP-1 co-localizes with RNA Pol II Ser5P as well as RNA Pol II Ser2P, we noted that co-localization co-efficiency of SHP-1 is significantly higher in CDK9 and RNA Pol II Ser5P in comparison to RNA Pol II Ser2P (Fig 5B), possibly suggesting an important role of SHP-1 during the early stages of transcription. Also, we found that SHP-1 readily interacts with the RNA Pol II and CDK9 in cells (Fig 5C). To further determine if SHP-1 is indeed required for cellular transcription, we analyzed the levels of active transcription marks upon loss of SHP-1. Interestingly, we found that deletion of SHP-1 in cells led to a significant reduction in RNA Pol II Ser2P levels coupled with RNA Pol II Ser5P accumulation (Fig 5D and Appendix Fig S4A). Furthermore, pharmacological inactivation of SHP-1 activity by treating cells with a specific inhibitor TPI also shows similar defects in active RNA Pol II (Fig 5E and Appendix Fig S4B). Importantly, the changes in RNA Pol II phosphorylation detected in SHP-1 KO cells could be rescued by expression of a non-phosphorylatable H2B Y121F mutant but not a phosphomimetic Y121D mutant (Fig 5F and Appendix Fig S4C). These data suggest that SHP-1 is required for transition of RNA Pol II into productive elongation stage from initiation phase of the transcription and loss of SHP-1 may lead to stalling of RNA Pol II at early phases of transcription. Moreover, reduced RNA Pol II Ser2P levels after SHP-1 deletion is associated with an overall reproducible and quantifiable decrease in the incorporation of 5-ethynyl uridine (EU) into nascent RNA detected by immunofluorescence staining (Fig 5G and H). Similar reduction in nascent RNA synthesis was also observed upon pharmacological inhibition of SHP-1 activity via TPI treatment (Fig 5I and J), thus suggesting that transcription elongation is attenuated across the transcriptome upon SHP-1 loss.

Loss of SHP-1 results in genome wide changes in H2B ubiquitination and pol II distribution

To gain more insights into how loss of SHP-1 impacts Pol II-dependent transcription and if SHP-1 coexists with RNAPII

transcription factories, we first determined the genome-wide occupancy of SHP-1 by chromatin immunoprecipitation (ChIP) coupled with deep sequencing. As no ChIP-grade antibodies were available for SHP-1 so far, we generated a rabbit polyclonal antibody for this purpose. Analysis of chromatin immunoprecipitate from MCF-7 cells demonstrated the proficiency of our antibody, albeit very weak, in specifically pulling down SHP-1 in ChIP experiments (Appendix Fig S5A). Our ChIP-Seq analysis revealed that SHP-1 is distributed across various regions of the genome (Appendix Fig S5B), however, predominantly at promoter (16%), first exon (22%) and distal intergenic regions (39%). Motif discovery analysis performed with the findMotifsGenome function of the HOMER retrieved several known and *de novo* motifs for SHP-1 binding (Appendix Fig S5C), suggesting a broad coverage of SHP-1 association across the genomic regions in cells with no bias for a particular transcription factor/site. Consistent with our observation that SHP-1 might be important during early events of Pol II-dependent transcription, we found that SHP-1 is highly enriched at the transcription start sites (Fig 6A and B). To further validate our ChIP-Seq data, we randomly picked two independent genes (SETD1A and SMARCE1) where SHP-1 has shown enrichment in the ChIP-Seq analysis (Appendix Fig S5D). Chromatin immunoprecipitation followed by q-RT-PCR analysis has clearly indicated that SHP-1 is readily enriched at the transcription start sites of these genes (Appendix Fig S5E), thus validating our SHP-1 ChIP-Seq data.

Furthermore, to understand how loss of SHP-1 impacts Pol II-dependent transcription, we analyzed H2B ubiquitination and Pol II occupancy at genome-wide level by performing ChIP-seq experiments in wild-type and SHP-1 knockout cells. Deletion of SHP-1 drastically reduced global H2B ubiquitination at the gene body (Fig 6C and D). Consistent with the role of H2Bub in regulating Pol II movement during transcription, reduction in global H2Bub in SHP-1 KO cells further led to alterations in Pol II occupancy at the coding regions (Fig 6E). SHP-1 knockout cells display significant enrichment of Pol II adjacent to TSS, suggesting impaired Pol II movement upon SHP-1 loss (Fig 6F). In fact, the pausing index

---

Figure 5. SHP-1 participates in Pol II-mediated transcription.

A   Representative super-resolution images of MCF7 cells immunostained with SHP-1 in combination with CDK9, total RNA Polymerase II, RNA polymerase II Ser2P, and RNA Polymerase II Ser5P. Scale bar: 5 μm. Fluorescence intensities along the line drawn in a representative section of cell were obtained using Zen software and the co-localization plots were made using GraphPad.

B   Co-localization of SHP-1 with CDK9, total RNA Polymerase II, RNA Polymerase II S2P, and RNA Polymerase II S5P was measured by Pearson correlation coefficient using ImageJ. Values are presented as the mean ± SD, *n* = 10 (from three independent experiments). ***P value <0.001. (One-way ANOVA).

C   Endogenous interaction of SHP-1 with RNA Polymerase II, RNA polymerase II Ser2P, and RNA Polymerase II Ser5P and CDK9 was detected by immunoblotting after performing immunoprecipitation with either IgG or SHP-1 antibody using TurboNuclease-treated cell lysate.

D   Nuclear extracts of MCF-7 WT and SHP-1 knockout cells were made and the levels of RNA Polymerase II, RNA Polymerase II Ser2P and RNA Polymerase II Ser5P were detected by immunoblotting using specific antibodies.

E   Nuclear extracts of cells treated with either DMSO or SHP-1 inhibitor TPI (50 nM) were used to detect total RNA Polymerase II and its modifications by immunoblotting using specific antibodies.

F   Nuclear extracts of MCF-7 WT and SHP-1 knockout cells transfected with Myc vector, H2B Y121F, or H2B Y121D constructs were made and the levels of RNA Polymerase II, RNA Polymerase II Ser2P, RNA Polymerase II Ser5P, and Lamin B1 were detected by immunoblotting using specific antibodies.

G   Immunofluorescence of WT or SHP-1 knockout MCF7 cells labeled with the 5-Ethynyl Uridine (EU) for 60 min to capture nascent RNA synthesis. Scale bars 10 μm.

H   The EU incorporation in MCF-7 WT and SHP-1 KO cells was quantified in three independent experiments. Values are presented as the mean ± SD, ***indicates *P* < 0.001 (One-way ANOVA).

I   Representative images of immunofluorescence of DMSO or TPI-treated (50 nM) MCF7 cells labeled with EU for 60 min are shown. Scale bar: 40 μm.

J   The EU incorporation in MCF7 cells treated with DMSO or TPI was quantified in three independent experiments. Values are presented as the mean ± SD, ***indicates *P* < 0.001 (One-way ANOVA).
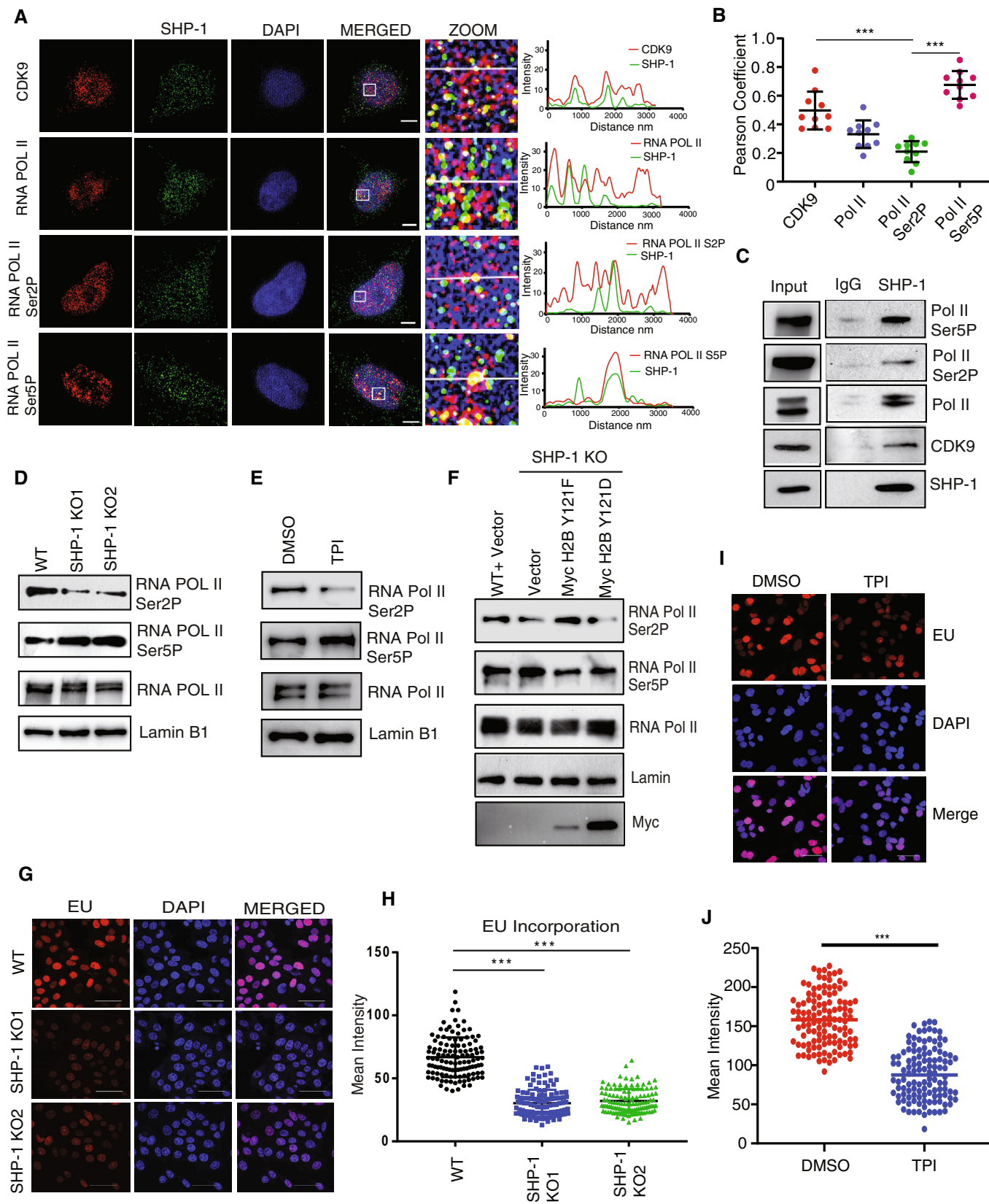
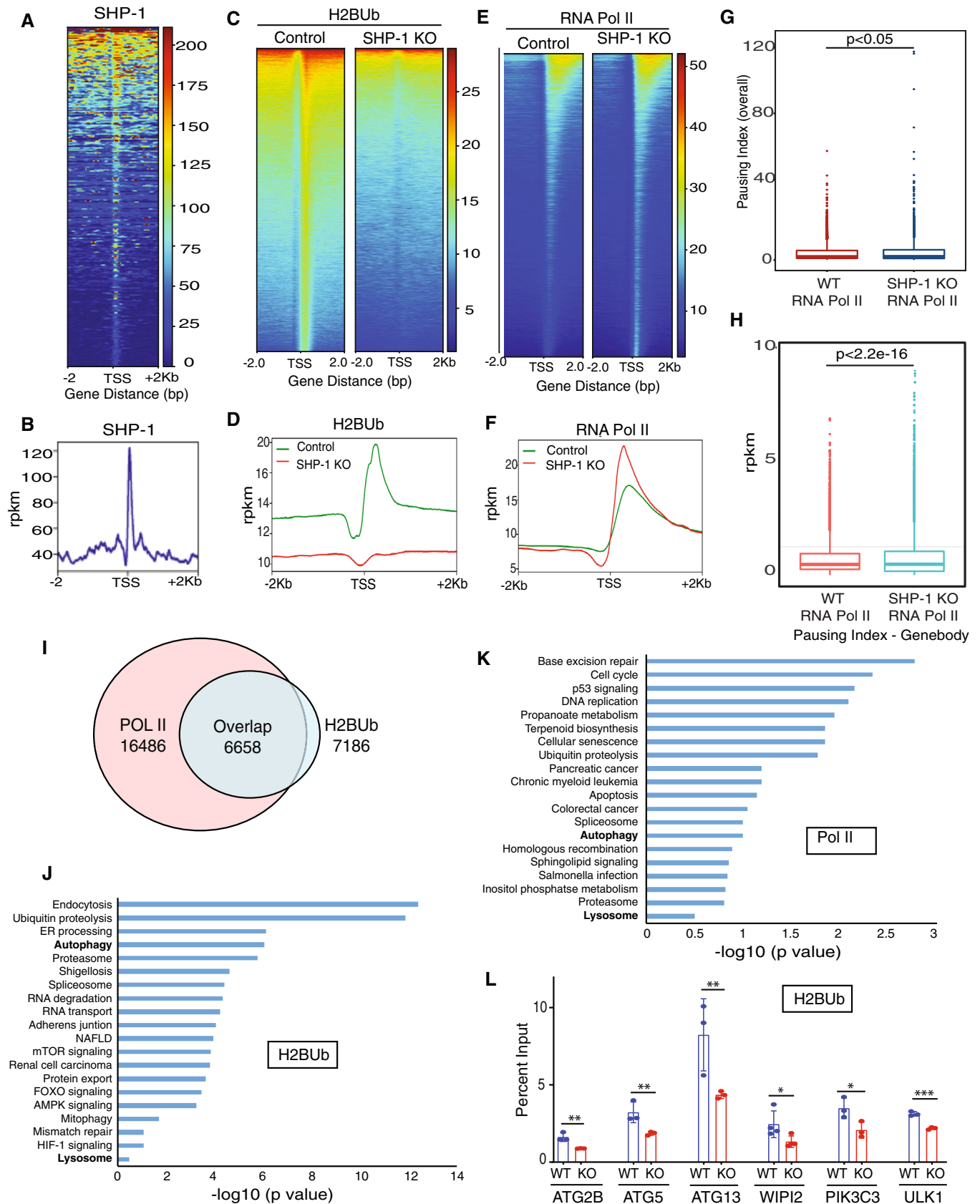Source data are available online for this figure.

Figure 5.

Figure 6.

◀

Figure 6. Deletion of SHP-1 leads to global changes in H2Bub and Pol II occupancy.

A   ChIP-seq density heatmap of SHP-1 occupancy within the extended gene regions (−2 kb to +2 kb around TSS) is shown.

B   Genome-wide enrichment profile for SHP-1 determined by ChIP Seq in MCF7 cells is shown (−2 kb to +2 kb around TSS).

C   Normalized ChIP-seq density heatmap of H2BUb occupancy over 2 kb upstream and downstream of TSS in SHP-1 WT and knockout MCF7 cells is shown.

D   Genome-wide H2Bub enrichment profiles around ± 2 kb TSS determined by ChIP-seq using H2Bub-specific antibodies in MCF7 WT, and SHP-1 KO cells are shown. Color-scaled intensities are in units of rpkm.

E   Heatmaps of the RNA Polymerase II occupancy around TSS (−2 kb to +2 kb) region determined by ChIP-seq using Pol II-specific antibodies in MCF7 WT and SHP-1 KO cells are shown. Heatmaps were ordered by descending ChIP-Seq signal intensity.

F   Genome-wide ChIP Seq density plot of RNA Polymerase II around the TSS in SHP-1 WT and knockout MCF7 cells is shown.

G, H   Box plot showing RNA Polymerase II (G) overall pausing index and (H) pausing index at gene body in MCF-7 WT and SHP-1 KO cells (n = 28,256 annotated regions). Data represent two independent experiments. Box represents overall signal distribution and line as the median. The upper and lower whiskers extend to the largest and smallest value, respectively. Significance was calculated using the Wilcoxon rank test.

I   Venn diagram showing number of distinct and common ChIP seq peak-associated genes from H2Bub and RNA Pol II ChIP-seq data in SHP-1 knockout cells.

J, K   Bar graphs showing the −log10 P-values of the most significant pathways enriched in (J) H2Bub ChIP-Seq and (K) Pol II ChIP-Seq derived from KEGG pathway analysis using Enrichr.

L   WT and SHP-1 knockout MCF7 cells were subjected to ChIP analysis using H2BUb antibody. H2BUb enrichment in the middle region of ATG2B, ATG5, ATG13, PIK3C3, WIPI2, and ULK1 with respect to WT is shown. The data shown are derived from three independent experiments. Error bars indicate the mean ± SD; **P < 0.01; *P < 0.05, one-way ANOVA.

measurements has confirmed that there is an overall Pol II stalling in SHP-1 KO cells (Fig 6G). Specifically, while pausing in the promoter regions was undetected (Appendix Fig S6A), we found significant Pol II pausing in the gene bodies of SHP-1 knockout cells (Fig 6H), suggesting that SHP-1 activity is necessary for transcription elongation. Analysis of H2Bub altered genes in SHP-1 KO cells revealed 92% overlap with genes having altered Pol II occupancy (Fig 6I), again strongly suggesting the dependency of Pol II activity on H2B ubiquitination in these cells. To further understand the functional significance of alterations caused by SHP-1 loss, we annotated the H2Bub (Fig 6J) and Pol II gene list (Fig 6K) with KEGG pathway. Analysis with Enrichr tool revealed genes associated with multiple cellular processes being affected by SHP-1 loss (Fig 6J and K). Although we found global changes in H2Bub and Pol II in SHP-1 KO cells, thereby focusing on specific cellular processes, we next sought to understand the physiological relevance of H2Bub and Pol II changes caused by SHP-1 loss in cells. Among the most significantly altered processes, interestingly, the genes associated with autophagy and lysosomes were commonly found to be affected in H2Bub and Pol II list. By analyzing a set of specific candidate gene loci associated with various steps of autophagy process (ATG2B, ATG5, ATG13, WIPI2, PIK3C3 and ULK1), we validated consistent reduction in H2Bub levels on these genes upon SHP-1 loss (Fig 6L and Appendix Fig S6B).

Next, we tested if SHP-1 is associated with these candidate gene loci. Indeed, chromatin immunoprecipitation with SHP-1 specific antibody followed by q-RT-PCR analysis has clearly indicated that SHP-1 is readily enriched at the transcription start sites of the autophagy-related genes (Fig 7A). Furthermore, reduced H2B ubiquitination at these gene loci followed by Pol II occupancy changes (Appendix Fig S6C) caused by SHP-1 loss led to their decreased gene expression (Fig 7B). Importantly, decrease in H2Bub levels at these gene loci in SHP-1 KO cells could be rescued by expression (Fig 7C) of a non-phosphorylatable H2B Y121F mutant, but not a phosphomimetic Y121D mutant (Fig 7D). Also, stalling of RNA Pol II at this autophagy-related gene loci (Fig 7E) and reduced expression of these genes (Fig 7F) in SHP-1 KO cells could be rescued by expression of a non-phosphorylatable H2B Y121F mutant, but not a phosphomimetic Y121D mutant. Therefore, these data fully support our hypothesis that SHP-1

participates in promoting H2B ubiquitination during transcription by dephosphorylating Y121 residue.

SHP-1-dependent H2B dephosphorylation is required for maintenance of basal autophagy

To further assess the functional role of SHP-1-dependent changes in the autophagy genes, we analyzed the autophagic process in MCF-7 breast epithelial cells (known to exhibit higher basal autophagy) (Gavilan et al, 2013). Consistent with defective gene expression, SHP-1 KO cells display reduced ability in the conversion of LC3-I to LC3-II (Fig 8A and B), suggestive of defective basal autophagy. Reduced conversion of LC3 is followed by significant accumulation of LC3 puncta in SHP-1 KO cells (Fig 8C and D). Furthermore, a significant accumulation of an autophagic cargo adaptor p62 in SHP-1 KO cells substantiated the role of SHP-1 in maintenance of autophagic flux in cells (Fig EV5A–C and Appendix Fig S7A). Interestingly, expression of wild-type SHP-1 with intact NLS, but not NLS mutant, rescues basal autophagy that was lost in SHP-1 knockout cells, suggesting that nuclear SHP-1 is required for the maintenance of autophagy (Fig 8E, Appendix Fig S7B, Fig EV5D and Appendix Fig S7C). On the other hand, H2B Y121F mutant, but not Y121D mutant, could reverse p62 levels (Fig 8F and G, EV5E, and Appendix Fig S7D) and defective LC3 conversion (Fig EV5F and Appendix Fig S7E) in SHP-1 KO cells, suggesting that SHP-1 maintains basal cellular autophagy via H2B dephosphorylation. Accumulation of LC3 and p62 in SHP-1 KO cells prompted us to propose two possibilities: firstly, the defective autophagosomes might have failed to fuse with lysosomes in these cells or, alternatively, the autophagic cargo is not efficiently degraded possibly due to defective lysosomes as well. We found that LC3 puncta co-localizes with LAMP2 and is significantly accumulated in lysosomes of SHP-1 KO cells (Fig 8H and I) compared to wild-type cells, thus supporting the second possibility of defective lysosomes. Indeed, in line with this hypothesis, we found that H2Bub levels were significantly reduced on multiple gene loci coding for lysosomal genes (Appendix Fig S8). Moreover, lysotracker staining suggested that SHP-1 KO cells has significantly reduced acidic lysosomes (Fig EV5G and H). Together, these data suggest that SHP-1 maintains basal autophagic flux by controlling various genes involved in multiple steps of autophagy and lysosomal pathways.
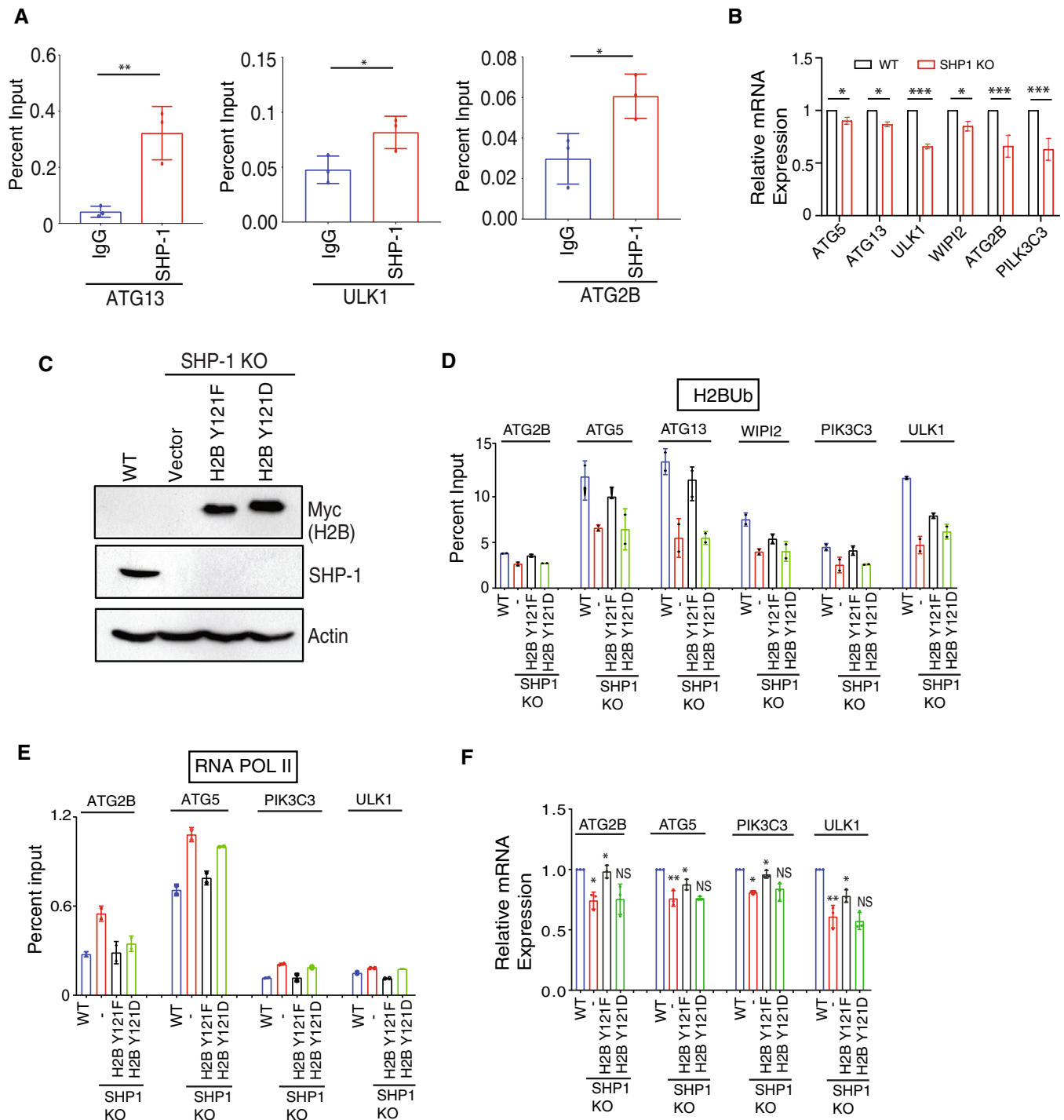
Figure 7. SHP-1 facilitates H2Bub and Pol II occupancy at transcriptional sites via H2B dephosphorylation.

A   ChIP-qPCR using either anti-IgG or anti-SHP-1 antibody was performed in MCF-7 cells and the binding of SHP-1 at TSS region adjacent to the promoter region of the ATG2B, ATG13, and ULK1 genes was determined. The Y-axis represents the percentage input signal. The data shown are derived from three independent experiments. Error bars indicate the mean ± SD; **$P < 0.01$; *$P < 0.05$, Student's t-test.

B   Expression of indicated genes in WT and SHP-1 knockout MCF7 cells was measured by qRT-PCR from three independent experiments. Values are presented as the mean ± SD. *$P < 0.05$ and ***P value <0.001, Student's t-test.

C, D   MCF-7 WT cells along with SHP-1 KO cells transfected with either vector, H2B Y121F, or H2B Y121D mutant were used for ChIP q-PCR analysis of the H2BUb at indicated genes. The data shown are derived from two independent experiments. Error bars indicate the mean ± SD.

E   MCF-7 WT cells along with SHP-1 KO cells transfected with either Myc vector, H2B Y121F or H2B Y121D mutant were used for ChIP-qPCR analysis of the RNA Pol II at indicated genes. The data are derived from two independent experiments. Error bars indicate the mean ± SD.

F   Expression of indicated genes in WT and SHP-1 knockout MCF7 cells transfected with Myc vector, Myc H2B Y121F, or Myc H2B Y121D mutant was measured by qRT-PCR from three independent experiments. Values are presented as the mean ± SD. *$P < 0.05$, **$P < 0.01$, one-way ANOVA.

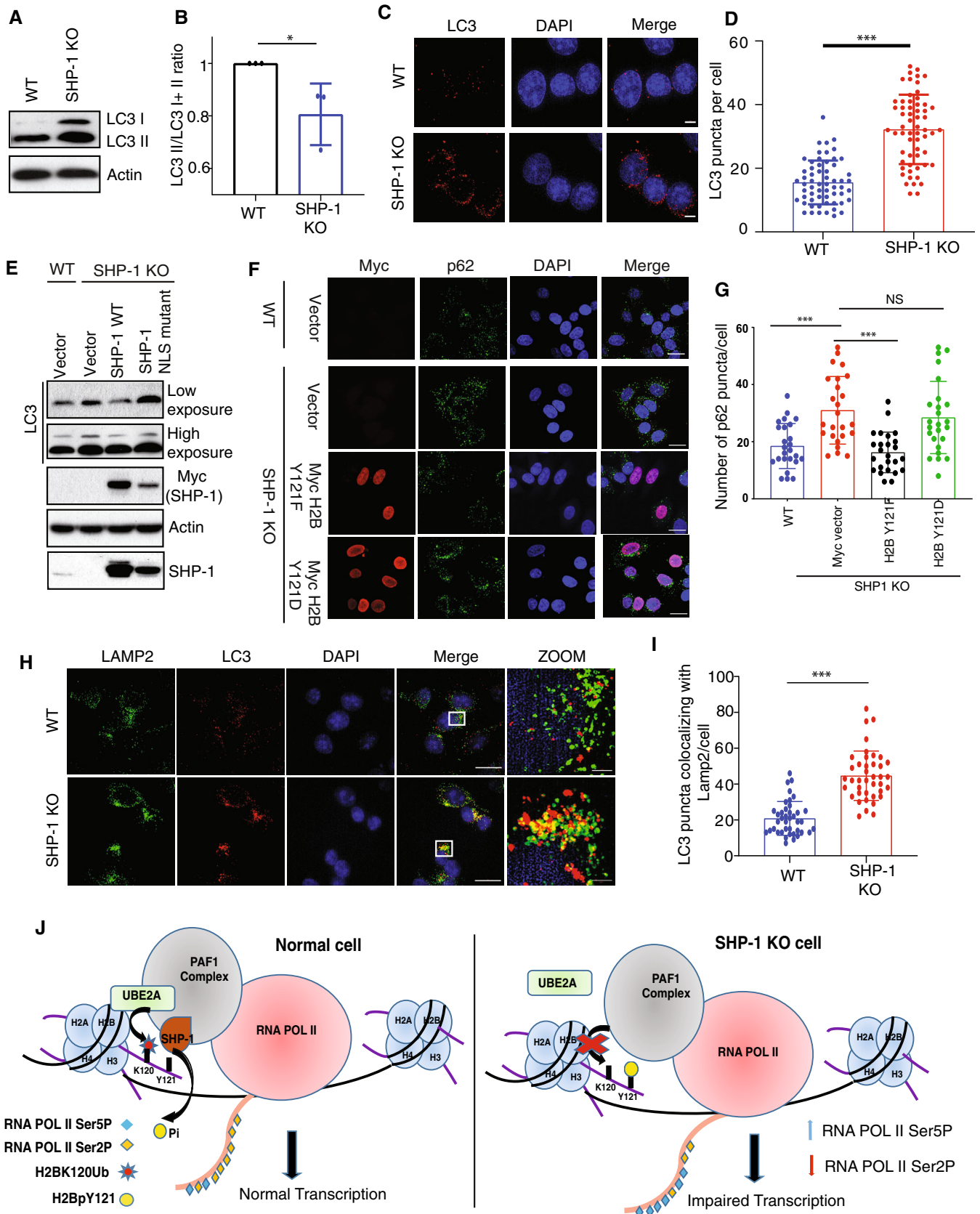**Figure 8.**

Figure 8. SHP-1 is required for maintenance of basal autophagic flux.

A   Lysates of WT and SHP-1 knockout MCF7 cells were made and the levels of LC3-I and II were detected by immunoblotting.

B   Levels of LC3 II were normalized against total LC3 (LC3 I + LC3 II). The data shown are derived from three independent experiments. Error bars indicate the mean ± SD. *P value < 0.05, Student's t-test.

C   Representative super-resolution images of WT and SHP-1 KO MCF7 cells immunostained with LC3 antibody, (Scale bar: 5 μm).

D   Quantification of LC3 puncta accumulation per cell done by using ImageJ is shown. Bars represent mean ± SD (N = 60). ***P value < 0.001, Student's t-test.

E   WT along with SHP-1 KO MCF7 cells transfected with either Myc vector, Myc SHP-1, or Myc SHP-1 NLS mutant were lysed. Levels of LC3 and actin were determined using specific antibodies.

F   WT and SHP-1 knockout MCF7 cells transfected with the Myc vector or Myc-tagged H2B, H2B Y121F, or H2B Y121D constructs were immunostained with endogenous p62 and Myc antibody. Image acquisition was done using LSM 700, (Scale bar: 20 μm).

G   Accumulation of p62 was quantified by counting p62 positive puncta per cell (N = 25); values are presented as the mean ± SD. ***P value < 0.001 (One-way ANOVA).

H   Representative super-resolution images of LC3 and LAMP2 immunostaining in WT and SHP-1 KO MCF7 cells. (Scale bar: 20 μm for merge and 5 μm for Zoom).

I   LC3 puncta co-localizing with LAMP2 per cell were quantified using ImageJ (N = 45); values are presented as the mean ± SD. ***P value < 0.001, Student's t-test.

J   A proposed model to depict the role of nuclear SHP-1 during active transcription. SHP-1 dephosphorylates H2B at Y121 residue, thereby allowing ubiquitination of K120 site and productive transcription. Loss of SHP-1 leads to impaired transcription as H2B stays in a constitutively phosphorylated state at Y121, thus precluding interaction of E2 enzyme and failure to ubiquitinate H2B.

Source data are available online for this figure.

Discussion

Histones are subjected to diverse posttranslational modifications such as phosphorylation, acetylation, methylation, ubiquitination, SUMOylation, ADP ribosylation, deamination, proline isomerization, serotonylation, and lactylation to provide dynamic environment for precise regulation of gene expression in eukaryotes (Shilatifard, 2006; Farrelly *et al*, 2019; Zhang *et al*, 2019). The list of these modifications is constantly growing and the intricacies of their functions are only just beginning to be understood. Identification of new histone modifications, specifically the tyrosine modifications, critical for transcriptional control has gained immense interest in recent years. So far, a handful of tyrosine modifications like H3pY41 (Dawson *et al*, 2009), H2ApY57 (Basnet *et al*, 2014), H2BY37 (Mahajan *et al*, 2012), and H4pY88 (Mahajan *et al*, 2017) are reported to have a positive role in genome-wide as well as context-dependent transcription. In this study, we identified a new histone tyrosine modification that acts as a regulatory switch during eukaryotic transcription. We found that phosphorylation on tyrosine 121 residue negatively influences transcriptional outcome by inhibiting covalent attachment of ubiquitin to adjacent K120 residue (H2Bub). Tyrosine phosphatase SHP-1 dephosphorylates Y121 and allows H2B ubiquitination, thereby permitting productive transcription (model shown in Fig 8J).

One of the important features of histone modifications is the existence of crosstalk between different modifications. The earliest examples of histone modification that promotes the generation of another modification on the same histone tail were observed in the budding yeast *Saccharomyces cerevisiae*. Phosphorylation of serine 10 (S10) on histone H3 by the Snf1 kinase promoted the Gcn5-mediated acetylation of H3 lysine 14 (K14) during gene activation (Cheung *et al*, 2000; Lo *et al*, 2000). Subsequently, several crosstalks between histone modifications have emerged (Suganuma & Workman, 2008). However, undoubtedly, there are more modifications and mechanisms of histone crosstalk to be discovered. In contrast to promoting another modification, histone modification crosstalks can also direct the loss of certain modifications. For instance, H3 lysine 36 (K36) methylation leads to the removal of acetyl groups from H3 and H4 (Lee & Shilatifard, 2007). In addition to the crosstalk between modifications on the same histone, some of the most exciting examples involve trans-histone effects, where

modifications on histone affect the modification of a different histone. Of specific interest is the role of H2B monoubiquitination in regulating multiple downstream modifications on other histones. H2B ubiquitination by the Rad6 enzyme is necessary to trigger H3 lysine 4 (H3K4) methylation by the Set1 methyltransferase subunit of the COMPASS complex and H3 lysine 79 (H3K79) methylation by the Dot1 methyltransferase, which is critical for transcriptional process (Zhu *et al*, 2005). Interestingly, however, an upstream regulatory event that participates in the cross talk with H2B ubiquitination is unknown so far. Therefore, our study identifying Y121 phosphorylation as an upstream control switch for H2B K120 ubiquitination adds another important layer of regulation during transcription.

Histone modifications in general exert their effects either by directly influencing the chromatin structure or by regulating (positively or negatively) the binding of downstream effector proteins. For example, phosphorylation of Histone H3 at S10 residue that occurs during mitosis leads to condensed chromatin (Wei *et al*, 1998). Similarly, modifications such as histone acetylation were also indicated to alter the chromatin structure under certain conditions (Bannister & Kouzarides, 2011). On the other hand, multiple examples exist wherein chromatin-associated proteins have been demonstrated to specifically interact with modified histones via distinct domains such as Tudor domain, Chromodomain, PHD fingers, and Bromodomain (Bannister & Kouzarides, 2011). It is possible that SHP-1 controlled H2B Y121 phosphorylation that we identified here might alter the chromatin structure at specific stages of transcription, thereby regulating the accessibility of effector proteins and the transcriptional machineries. Identification of differential binding partners using the phosphorylated versus non-phosphorylated H2B at Y121 residue, which is being actively pursued in the lab, may provide us further clues on how Y121 phosphorylation/dephosphorylation cycle alters the downstream processes. Furthermore, to fully appreciate the role of H2B Y121 phosphorylation during specific steps of transcription, it is important to map the landscape of Y121 phosphorylation at the genomic level, in future studies.

While here we demonstrated the functional significance of SHP-1-dependent H2B dephosphorylation during regulation of autophagic gene expression, it is quite clear from our H2Bub and Pol II ChIP-seq data that SHP-1 may participate in regulation of several other cellular processes. To understand the role of chromatin-

bound SHP-1:H2B connection in different cellular processes, it is imperative to identify and map the binding regions of SHP-1 on various genes known to be involved in these cellular processes. Non-availability of ChIP grade antibodies for SHP-1 is a limitation in this process. Although we utilized a custom-generated polyclonal antibody to demonstrate the association of SHP-1 at TSS regions of certain genes, we believe that genomic coverage for SHP-1 binding is low due to poor efficiency of the antibody. Therefore, generation of a high-quality ChIP grade monoclonal SHP-1 antibody is essential to fully appreciate the functional repertoire of chromatin-associated SHP-1 in cells. In addition to its role in transcription, H2Bub has been demonstrated to have an important role in events such as DNA damage response and repair, maintenance of genome stability, and tumorigenesis (Meas & Mao, 2015). Given that H2B Y121 phosphorylation controls H2B ubiquitination, it would be interesting to test if Y121 phosphorylation participates in these processes as well. Interestingly, SHP-1, the enzyme that we have shown to control Y121 phosphorylation, displays aberrations in different human cancers. For example, due to promoter hypermethylation, SHP-1 expression is reduced in the hematological malignancies like lymphoma and leukemia (Zhang et al, 2000). On the contrary, increased SHP-1 levels were detected in a subset of breast and in ovarian cancers (Yip et al, 2000). Thus, we speculate that there might be important roles of H2B Y121 phosphorylation in human cancers, which need to be unveiled in future studies.

Materials and Methods

Plasmids, shRNAs, and guide RNA

cDNA of SHP-1, Paf1, LEO1, CDC73, CTR9, WDR61, RTF1 and UbE2A were purchased from Dharmacon. H2B plasmid was purchased from addgene. All cDNAs were PCR amplified and cloned into SFB (S protein tag, FLAG tag, streptavidin-binding protein tag) triple tagged destination vector using gateway cloning. All clones were verified by sequencing. SHP-1 and H2B were cloned into Myc, MBP and GST destination vectors using the same cloning system. Point mutants (H2B Y37F, Y41F, Y43F, Y83F Y121F, Y37D, Y41D, Y43D, Y83D, Y121D, K120R) for H2B, SHP-1 ΔSH2 (comprising residues 248–597), SHP-1 C453S, SHP-1 NLS mutant (595 KRK597 mutated to AAA) were generated by site-directed mutagenesis and cloned into SFB, Myc, GST, and MBP-tagged destination vectors. Lentiviral-based shRNAs for SHP-1, Paf1, LEO1, CDC73, CTR9, WDR61, and RTF1 were purchased from open biosystems. Lentiviral vectors coding SHP-1 guide RNAs were purchased from transOMIC technologies inc.

Antibodies

Following antibodies were used in this study: SHP-1 (Abcam ab32559, WB 1:1,000), SHP-1 (Biolegend 620301, IF 1:200), SHP-1 (Bioklone, IP 2 µg), pY121-H2B (Bioklone, WB 1:50), RNA Polymerase II S2P (Abcam ab5095, WB 1:5,000 and IF 1:200), RNA Polymerase II S5P (ab5131, WB 1:5,000 and IF 1:200), RNA Polymerase II (CST 14958, WB, ChIP), RNA Polymerase II (Santa Cruz Biotechnologies sc9001; IF 1:100, Paf1 (CST 12883, WB 1:1,000), Leo1

(Bethyl A300-174A, WB 1:500), CTR9 (Bethyl A301-395A, WB 1:1,000), RTF1(Bethyl A300-179A, WB 1:1,000), WDR61(Bethyl A305-191A, WB 1:1,000), CDC73 (Novus NB200-184, WB 1:5,000), FLAG (Sigma F3165, WB 1:10,000), Actin (Sigma A5441; WB 1:10,000), Lamin B1(Abcam Ab16048 WB 1:5,000), Syk (CST 13198, WB 1:1,000), GST (Santa Cruz Biotechnologies, WB 1:5,000), HIS (Bethyl, WB 1:1,000), MBP (NEB, WB 1:5,000), Myc-tag (Santa Cruz Biotechnologies. WB 1:1,000), H2B (Millipore 07–371, WB 1:5,000); H2B (Abcam ab52484, 5 µg for endogenous IP), H2B ubiquitylated at Lys120 (H2BUb; CST 5546, WB 1:1,000), Anti p62 (CST 5114, WB 1:2,000); Abcam ab56416, IF 1:200), Anti Tubulin (Sigma T6074, WB 1:1,000), Phospho tyrosine (CST 9416, WB 1:1,000), CDK9 (Santa Cruz Biotechnologies, IF 1:100), LC3B (CST 83506, WB 1:5,000 and CST 4108, IF 1:200), LAMP2 (DSHB GL2A7 IF 1:200), Histone H4 (Abcam Ab10158, WB 1:5,000), H2A (Abcam Ab177308, WB 1:1,000), UbE2A (Bethyl A300-281A, WB 1:5,000), Myc Tag (Abcam ab9106, IF 1:200). Polyclonal anti-SHP-1 antibodies were raised by immunizing rabbits with GST-SHP-1 fusion protein (Bioklone, India). Antisera were affinity-purified using Amino Link plus Immobilization and purification kit (ThermoFisher). Antibodies for H2B-pY121 were generated by immunizing rabbits with a peptide having phosphate at Y121 position (KAVTK(pY)TSAK). After clearing through non-phospho peptide (KAVTKYTSAK) column, antibodies were affinity-purified using the column immobilized with the phospho-peptide.

Cell lines and transfections

MCF7, MDA-MB 231, HEK 293T, HCT116, A549, HeLa, THP-1, Jurkat, U937, RPE1, MCF10A and BOSC23 cell lines were used in this study. Except, MCF7, MCF10A and MDA-MB 231 cells, all cells were grown in RPMI containing 10% donor bovine serum (DBS) and 1% penicillin and streptomycin. MCF7 and MDA-MB-231 cells were maintained in DMEM plus 10% DBS with 1% penicillin and streptomycin. MCF10A cells were maintained in DMEM/F12 medium supplemented with 5% FBS, 20 ng/ml EGF, 0.5 mg/ml hydrocortisone, 100 ng/ml cholera toxin, 10 µg/ml insulin along with penicillin and streptomycin. Cells were continuously checked by microscopy for their original morphology and tested for mycoplasma contamination by using DAPI staining. Transfection of cells with different plasmids was carried out with PEI (Polysciences) according to the manufacturer's protocol. Briefly, the plasmid diluted in serum-free RPMI medium was mixed with PEI (1 mg/ml) in 1:3 ratio. After incubating the DNA–PEI mixture at room temperature for 15 min, the complexes were added to cells to allow the transfection of plasmid.

Lentiviral infection

Lentivirus-based Paf1, RTF1, and CTR9 shRNA clones were purchased from Open Biosystems. shRNAs were transfected transiently using PEI (Invitrogen) in BOSC23 packaging cells along with packaging vectors (psPAX2 and pMD2.G); 48 h post transfection, the viral medium was collected, filtered through 0.45 µM filter, and added to the target cells along with polybrene (8 mg/ml); 72 h post infection, cells were collected and processed for various assays and immunoblotting was performed with the specific antibodies to check the efficiency of knockdown.

Generation of SHP-1 knockout cell lines

SHP-1 knockout MCF7 and 293T cell lines were established using the CRISPR/Cas9 system. In brief, guide RNAs (TEVH-1119886 and TEVH-1187028) targeting SHP-1 and non-targeting control (TELA1011) were purchased from transOMIC technologies (pCLIP-All-EFS-Puro vector). Plasmids were transfected into cells with Turbofect according to the manufacturer's protocol. After 48 h, cells were treated with puromycin (2 µg/ml) and further subjected to clonal selection. Positive clones were verified by Western blot for the absence of SHP-1 protein expression.

Immunoprecipitation

For immunoprecipitation assays, cells were harvested and lysed with NETN buffer (20 mM Tris- HCl at pH 8.0, 100 mM NaCl, 1 mM EDTA, 0.5% Nonidet P-40) containing 1 mg/ml each of pepstatin A and aprotinin, centrifuged at 13,000 rpm for 15 min at 4°C. The whole-cell lysates obtained by centrifugation were incubated with 5 µg of specific antibody bound to protein G sepharose beads for 4 h at 4°C. TurboNuclease (50 U/ml) treatment for 30 min in the presence of 1 mM $MgCl_2$ was carried out on cell lysates before immunoprecipitation in specific experiments to rule out the interference from DNA contamination during protein–protein interactions. The immunocomplexes were then washed with NETN buffer six times and eluted by boiling in 1× laemmli buffer. Samples were resolved by SDS-PAGE and immunoblotted with indicated antibodies.

Denaturing immunoprecipitation

The 293T whole cell lysate was prepared by boiling the cells in denaturing lysis buffer (20 mM Tris pH 8.0, 1% SDS, 10 mM dithiothreitol) for 10 min. The SDS concentration of cell lysate was adjusted to 0.1% by adding 1× NETN buffer and incubated on ice for 20 min. The whole-cell lysates obtained by centrifugation were incubated with streptavidin–sepharose for 4 h at 4°C. The immunocomplexes were then washed with NETN buffer six times and applied to SDS–PAGE.

Peptide competition assay

To validate the specificity of Y121 phospho antibody, the peptide competition experiment was performed according to the following protocol (http://docs.abcam.com/pdf/protocols/peptide_competition_assay_protocol.pdf). Briefly, 2 µg of primary antibody (pY121 specific antibody) was left with no peptide or incubated with 100 µM of either non-phospho or phospho-peptide of H2B for overnight. The pre-incubated antibody in each of these samples was used in immunblotting of nuclear cell lysates to detect Y121 phosphorylation signal.

In vitro ubiquitination assay

In vitro ubiquitination assay was performed according to the protocol described earlier (Kim & Roeder, 2011; Yao *et al*, 2015). Briefly, ubiquitination reactions containing 100 ng E1, 100 ng E2, 2.5 µg ubiquitin, and 2.0 µg recombinant WT H2B, H2B Y121F, or H2B Y121D mutants or 1 µg of phospho or non-phosphopeptides or 2 µg His H2A: H2B, His H2A: H2BY121F and His H2A: H2B dimers in 20 µl reaction buffer (50 mM Tris–HCl pH 7.9, 5 mM $MgCl_2$, 2 mM NaF, 0.4 mM DTT, and 4 mM ATP) was incubated at 37°C for 1.5 h and then subjected to SDS–PAGE and Western blot using the H2BK120Ub antibody.

H2A: H2B Dimer preparation

H2A: H2B dimers were prepared as described earlier (Tachiwana *et al*, 2008). *Escherichia coli* BL21 (DE3) cells producing His H2A, His H2B, His H2B Y121F, and His H2B Y121D were collected and suspended in buffer containing 50 mM Tris pH 8, 500 mM NaCl, 1 mM PMSF, and 5% glycerol. Samples were sonicated for 20 cycles in Diagenode Bioruptor at high power (30 s on 30 s off). After centrifugation at 27,000 *g* for 20 min at 4°C, the pellets containing His tagged histones were re-suspended in urea buffer (Tris pH 8, 6 M Urea) and cleared by centrifugation at 27,000 *g* for 20 min at 4°C. Cell lysates were pulled down with Ni-NTA beads for 1 h at 4°C. The beads were then washed with a urea buffer containing 5 mM imidazole and bound proteins were eluted with the tris-urea buffer containing 300 mM imidazole. His tagged H2A and H2B proteins were mixed in the equimolar ratio in tris-urea buffer and dialyzed overnight against reconstitution buffer (20 mM Tris pH 8, 5 mM DTT, 1 mM EDTA, 1 mM PMSF, and 5% glycerol) containing 2 M NaCl. To lower the concentration of NaCl, stepwise dialysis was performed against the reconstitution buffer (1 M NaCl for 4 h, 0.5 M NaCl for 4 h and 0.1 M NaCl overnight) at 4°C. After dialysis, samples were cleared by centrifugation at 27,000 *g* for 10 min to remove insoluble aggregates.

Micrococcal nucleosome preparation

Nucleosomes were prepared as described earlier (Khan *et al*, 2020). Briefly, cells were harvested by centrifugation at 4°C for 5 min at 300 *g*, washed twice with ice-cold PBS and once with buffer A (10 mM HEPES pH 8, 10 mM KCl, 1.5 mM $MgCl_2$, 340 mM sucrose, 10% glycerol, and 1 mM DTT). Cells were resuspended in buffer A containing 0.2% Triton-X100 and incubated on ice for 5 min. The nuclei were pelleted by centrifugation (1,300 *g*, for 5 min, at 4°C) and washed once with ice-cold buffer A, followed by centrifugation (1,300 *g*, 5 min at 4°C). Then, nuclei were digested with 40 units/ml micrococcal nuclease (NEB) in digestion buffer (15 mM NaCl, 60 mM KCl and 10 mM $CaCl_2$) for 2 h at 37°C. The micrococcal nuclease reaction was quenched by the addition of EGTA to a final concentration of 20 mM. Then, samples were centrifuged at 13,000 *g* for 5 min at 4°C. The supernatant containing soluble nucleosomes was collected and stored at −80°C before use. The quality of the purified nucleosomes was analyzed by gel electrophoresis.

Immunofluorescence staining

Cells were grown on glass coverslips and fixed with 3% paraformaldehyde solution in PBS at room temperature for 10 min. Permeabilization of the cells was carried out with ice-cold methanol for 10 min and cells were incubated with 5% BSA for blocking at room temperature for 60 min. After this step, cells were washed

with PBS and incubated with primary antibodies overnight at 40C followed by washing thrice with 1× PBS. Cells were then incubated with Alexa488 or rhodamine-conjugated secondary antibodies at 37°C for 60 min followed by washing thrice with 1× PBS. Nuclei were stained with 4′,6-diamidino-2-phenylindole (DAPI). After a final wash with PBS, coverslips were mounted with glycerin-containing para- phenylenediamine, and imaging was done using a confocal microscope (LSM Meta 510, Zeiss). For LC3 and LAMP2 staining, cells were fixed with ice-cold methanol for 10 min and 4% paraformaldehyde fixative was used for p62 staining as well as lyso-tracker staining. Super-resolution images were acquired with LSM 980 Airyscan 2 microscope using Plan-Apochromat 63×/1.4 Oil DIC M27. Images were obtained using Z-stacks with a step size of 0.5 μm. Raw images were processed using the Zen Black software.

Histone extraction

Histone extraction was performed according to the protocol described earlier (Shechter *et al*, 2007). Briefly, cells were collected in 1× PBS and lysed in hypotonic lysis buffer to obtain nuclei. Histones were extracted by incubating nuclear pellets in 0.4 N H_2SO_4 overnight at 4°C. The supernatant containing histones was precipitated using chilled trichloroacetic acid (33%). The precipitate was washed with acetone to remove residual TCA. The pellets were air dried and 1× NETN was added to dissolve histones. Histone fractions were subjected to SDS-PAGE followed by Western blotting with antibodies of interest.

Subcellular fractionation

After washing twice with ice cold PBS, the cell pellets were resuspended in CE buffer (20 mM Tris, pH 7.6, 50 mM ß-mercaptoethanol, 0.1 mM EDTA, 2 mM $MgCl_2$, 1 mM PMSF supplemented with protease and phosphatase inhibitors) and incubated for 2 min at room temperature and for another 10 min on ice. After incubation, NP-40 was added at a final concentration of 1% (v/v) and lysates were homogenized by passing through a 22-G needle for three times. Nuclei were pelleted by centrifugation at 600 *g* for 5 min at 4°C and supernatant containing cytoplasmic fraction was collected. The remaining nuclei pellets were washed three times in CE buffer containing 1% NP-40. The nuclear pellets were lysed in NE buffer (20 mM HEPES, pH 7.9, 2.5% glycerol, 1 mM EDTA, 0.4 M NaCl, 1 mM PMSF, 10 mM NaF, 2 mM Na_3VO_4, 0.5 mM DTT, supplemented with protease inhibitors) by repeated freezing and thawing. Supernatant containing soluble nuclear fraction was collected by centrifugation at 20,000 *g* for 20 min. The chromatin pellets obtained following centrifugation were resuspended in SDS loading dye and boiled for 10 min at 90°C.

In vitro phosphatase assay

The bacterially purified H2B was incubated in the presence of 0.1 μg Syk and 10 μM ATP in reaction buffer (30 mM HEPES pH 7.5, 2 mM $MnCl_2$, 10 mM $MgCl_2$, 2 mM DTT and 0.1 mM Sodium Orthovandate) at 30°C for 60 min. For the kinase reaction on Paf1 components, bacterially purified proteins were incubated with 293T lysate in the presence of 25MM HEPES (pH 7.5), 25 mM ß-glycerophosphate, 25 mM $MgCl_2$, 2 mM DTT, 0.1 mM sodium orthovandate, and 1 mM ATP. The phosphorylated substrates were then incubated with constitutively active mutant (SHP-1 ΔSH2) or catalytically inactive mutant (SHP-1 C/S) in reaction buffer (25 mM HEPES pH 7.4, 2.5 mM EDTA, 5 mM DTT, and 50 mM NaCl) at 37°C for 60 min. After phosphatase assay, beads were washed three times with 1× NETN and run on SDS-PAGE followed by transfer onto PVDF membrane. After incubating the membrane with blocking buffer (1 h), pIMAGO-Biotin reagent was added and further incubated for 1 h. After three washes with 1× wash buffer, the membrane was incubated with avidin-HRP for 1 h. After washing three times with 1× TBST, phosphorylation signals were detected by ECL reagent. On the other hand, the released phosphate was also detected using malachite green assay kit (Cayman) by measuring the absorbance at 620 nm.

In vitro binding assay

Bacterially expressed GST–H2B or control GST immobilized to Glutathione-Sepharose beads (GE Healthcare) was incubated with bacterially purified MBP SHP-1 for 2 h at 4°C. Further beads were washed five times and the washed complexes were eluted by boiling in 2× SDS sample buffer and then separated by SDS–PAGE; the interactions were analyzed by Western blotting.

EU incorporation and IF

SHP-1 WT and knockout MCF7 cells were incubated with a modified nucleotide Ethynyl Uridine (EU) at 2 mM concentration for 30 min for incorporation into nascent RNA prior to fixation. Detection with the Click-iT RNA Alexa Fluor 594 Imaging Kit (Thermo Fisher, C10330) was done according to the manufacturer's instructions. Image acquisition was done using Leica SP8.

Quantitative real-time PCR

Total RNA was isolated using Macherey-Nagel RNA isolation kit as per the manufacturer's instructions. Reverse transcription was performed using cDNA synthesis kit (Takara). qRT-PCR was then performed using the TB Green Premix Ex Taq II (Tli RNaseH plus) kit (Takara Bio) in Biorad real-time PCR systems as per the manufacturer's protocol. The threshold cycle (Ct) values for particular genes were normalized to GAPDH for each sample. Sequences for primers used for qRT-PCR analysis are included in Appendix Table S1.

ChIP assay

The 3 μg rabbit IgG (Bethyl Laboratories), 4 μl of H2BUb (CST 5546; dilution 1:200), 4 μl (RNA Polymerase II; CST 14958) or 20 μl of SHP-1 (In house purified) antibodies were used for chromatin immunoprecipitation (ChIP) assay. Briefly, MCF7 cells were cross-linked with 1% formaldehyde for 10 min at room temperature. Crosslinking was quenched by the addition of glycine to a final concentration of 125 mM. Cells were then spun down and washed twice with ice-cold 1 × PBS and lysed in cell lysis buffer (5 mM PIPES pH 8.8, 5 mM KCl, 0.5% NP-40, and protease inhibitors) followed by nuclei lysis buffer (50 mM Tris pH 8.1, 10 mM EDTA, 1% SDS, and protease inhibitors). Isolated chromatin was sheared to a range of 500–200 bp by sonicating for 20 cycles (30 s on, 30 s off)

using a Diagenode Bioruptor at medium power. After centrifugation, the supernatant was diluted with 1 × IP dilution buffer and preclearing was performed using Protein G beads for 1 h. Then, equal amount of antibody was added and incubated on a nutator overnight at 4°C. Next day, protein G beads were added to chromatin. Beads were washed twice with IP Dialysis buffer (2 mM EDTA and 50 mM Tris pH 8) and three times with IP wash buffer (100 mM Tris pH 8, 250 mM LiCl, 1% NP-40, and 1% Na deoxycholate) for 5 min at room temperature. Then, beads were quickly washed with 1 × TE and bound DNA fragments were eluted twice using elution buffer (50 mM $NaHCO_3$ and 1% SDS) at 65°C. Input and eluted DNA was heated at 65°C overnight for reverse crosslinking which was followed by RNase treatment and finally the proteinase K treatment. DNA samples were purified using Phenol Chloroform extraction method.

ChIP-seq analysis

The ChIP DNA (10 ng) was used for making ChIP-sequencing libraries using NEB Next Ultra II DNA Library preparation kit. Paired-end sequencing (2 × 100 bp) was performed on the Illumina HiSeq 2500/4000 for H2Bub and RNA Pol II ChIP Seq and Illumina Nextseq 2000 platform for SHP1 ChIP Seq. Fastqc of chip-seq data was done using babraham fastqc tools (https://www.bioinformatics.babraham.ac.uk/projects/fastqc/). Bowtie2 (version 2.3.2) was used to perform alignment of the respective paired-end samples using hg38 reference genome. Sorting and indexing of bam files were done using samtools (version 1.9). Duplicate reads were removed using picard tool (version 2.9.4). To generate the matrix for genomic regions and heatmaps, Deeptool functions "computeMatrix" and "plotheatmap" were used. Macs2 (version 2.2.7.1) was used for peak calling of respective samples. Those peaks were filtered for the blacklist region using hg38-blacklist.v2.bed, which was obtained from the ENCODE consortium. Bedops (version 2.4.27) was used for overlaping genomic regions. The "annotatePeaks.pl" and "analyzerepeats.pl" scripts from HOMER suite (version 4.6) (using gencode hg38) were used to annotate peaks and to calculate the pausing index for RNA polymerase II datasets. Statistical analysis was performed in R (version 3.6.0) using "ggpubr" library (version 0.4.0) along with ggplot2 (version 3.3.3).

Data availability

ChIP seq data for H2Bub, RNA Pol II, and SHP-1 are available at array express (E-MTAB-10295). https://www.ebi.ac.uk/arrayexpress/experiments/E-MTAB-10295/

Expanded View for this article is available online.

Author contributions
Prajakta Tathe: Data curation; formal analysis; investigation; methodology; writing – original draft; writing – review and editing. **K V S Rammohan Chowdary:** Investigation; methodology. **Krushna Chandra Murmu:** Data curation; formal analysis; methodology. **Punit Prasad:** Data curation; formal analysis; methodology. **Subbareddy Maddika:** Conceptualization; resources; formal analysis; funding acquisition; writing – original draft; project administration; writing – review and editing.

In addition to the CRediT author contributions listed above, the contributions in detail are:
SM conceptualized and managed the project. SM and PT designed the experiments, analyzed the data, and wrote the manuscript. PT performed most of the experiments; KVSRC contributed to Paf complex interaction experiments. KCM and PP analyzed the ChIP-Seq data and also contributed to writing of the manuscript.

Disclosure and competing interest statement
The authors declare that they have no conflict of interest.

References

Azoulay-Alfaguter I, Strazza M, Peled M, Novak HK, Muller J, Dustin ML, Mor A (2017) The tyrosine phosphatase SHP-1 promotes T cell adhesion by activating the adaptor protein CrkII in the immunological synapse. *Sci Signal* 10: eaal2880

Bannister AJ, Kouzarides T (2011) Regulation of chromatin by histone modifications. *Cell Res* 21: 381–395

Bartkowiak B, Liu P, Phatnani HP, Fuda NJ, Cooper JJ, Price DH, Adelman K, Lis JT, Greenleaf AL (2010) CDK12 is a transcription elongation-associated CTD kinase, the metazoan ortholog of yeast Ctk1. *Genes Dev* 24: 2303–2316

Basnet H, Su XB, Tan Y, Meisenhelder J, Merkurjev D, Ohgi KA, Hunter T, Pillus L, Rosenfeld MG (2014) Tyrosine phosphorylation of histone H2A by CK2 regulates transcriptional elongation. *Nature* 516: 267–271

Brockdorff J, Williams S, Couture C, Mustelin T (1999) Dephosphorylation of ZAP-70 and inhibition of T cell activation by activated SHP1. *Eur J Immunol* 29: 2539–2550

Chen FX, Smith ER, Shilatifard A (2018) Born to run: control of transcription elongation by RNA polymerase II. *Nat Rev Mol Cell Biol* 19: 464–478

Chen F, Liu B, Guo L, Ge X, Feng W, Li DF, Zhou H, Long J (2021) Biochemical insights into Paf1 complex-induced stimulation of Rad6/Bre1-mediated H2B monoubiquitination. *Proc Natl Acad Sci USA* 118: e2025291118

Cheung P, Tanner KG, Cheung WL, Sassone-Corsi P, Denu JM, Allis CD (2000) Synergistic coupling of histone H3 phosphorylation and acetylation in response to epidermal growth factor stimulation. *Mol Cell* 5: 905–915

Core LJ, Waterfall JJ, Lis JT (2008) Nascent RNA sequencing reveals widespread pausing and divergent initiation at human promoters. *Science* 322: 1845–1848

Craggs G, Kellie S (2001) A functional nuclear localization sequence in the C-terminal domain of SHP-1. *J Biol Chem* 276: 23719–23725

Dawson MA, Bannister AJ, Gottgens B, Foster SD, Bartke T, Green AR, Kouzarides T (2009) JAK2 phosphorylates histone H3Y41 and excludes HP1alpha from chromatin. *Nature* 461: 819−822

Dustin LB, Plas DR, Wong J, Hu YT, Soto C, Chan AC, Thomas ML (1999) Expression of dominant-negative src-homology domain 2-containing protein tyrosine phosphatase-1 results in increased Syk tyrosine kinase activity and B cell activation. *J Immunol* 162: 2717−2724

Ebmeier CC, Erickson B, Allen BL, Allen MA, Kim H, Fong N, Jacobsen JR, Liang K, Shilatifard A, Dowell RD et al (2017) Human TFIIH kinase CDK7 regulates transcription-associated chromatin modifications. *Cell Rep* 20: 1173−1186

Farrelly LA, Thompson RE, Zhao S, Lepack AE, Lyu Y, Bhanu NV, Zhang B, Loh YE, Ramakrishnan A, Vadodaria KC et al (2019) Histone serotonylation is a permissive modification that enhances TFIID binding to H3K4me3. *Nature* 567: 535−539

Fuda NJ, Buckley MS, Wei W, Core LJ, Waters CT, Reinberg D, Lis JT (2012) Fcp1 dephosphorylation of the RNA polymerase II C-terminal domain is required for efficient transcription of heat shock genes. *Mol Cell Biol* 32: 3428−3437

Gates LA, Foulds CE, O'Malley BW (2017) Histone marks in the 'driver's seat': functional roles in steering the transcription cycle. *Trends Biochem Sci* 42: 977−989

Gavilan E, Sanchez-Aguayo I, Daza P, Ruano D (2013) GSK-3beta signaling determines autophagy activation in the breast tumor cell line MCF7 and inclusion formation in the non-tumor cell line MCF10A in response to proteasome inhibition. *Cell Death Dis* 4: e572

Hsin JP, Manley JL (2012) The RNA polymerase II CTD coordinates transcription and RNA processing. *Genes Dev* 26: 2119−2137

Jiang M, Zheng C, Shou P, Li N, Cao G, Chen Q, Xu C, Du L, Yang Q, Cao J et al (2016) SHP1 regulates bone mass by directing mesenchymal stem cell differentiation. *Cell Rep* 17: 2161

Khan KA, Ng MK, Cheung P (2020) The use of Mononucleosome immunoprecipitation for analysis of combinatorial histone post-translational modifications and purification of nucleosome-interacting proteins. *Front Cell Dev Biol* 8: 331

Kim J, Roeder RG (2011) Nucleosomal H2B ubiquitylation with purified factors. *Methods* 54: 331−338

Kim K, Kim JM, Kim JS, Choi J, Lee YS, Neamati N, Song JS, Heo K, An W (2013) VprBP has intrinsic kinase activity targeting histone H2A and represses gene transcription. *Mol Cell* 52: 459−467

Komarnitsky P, Cho EJ, Buratowski S (2000) Different phosphorylated forms of RNA polymerase II and associated mRNA processing factors during transcription. *Genes Dev* 14: 2452−2460

Kumar P, Munnangi P, Chowdary KR, Shah VJ, Shinde SR, Kolli NR, Halehalli RR, Nagarajaram HA, Maddika S (2017) A human tyrosine phosphatase Interactome mapped by proteomic profiling. *J Proteome Res* 16: 2789−2801

Lee JS, Shilatifard A (2007) A site to remember: H3K36 methylation a mark for histone deacetylation. *Mutat Res* 618: 130−134

Li B, Carey M, Workman JL (2007) The role of chromatin during transcription. *Cell* 128: 707−719

Lo WS, Trievel RC, Rojas JR, Duggan L, Hsu JY, Allis CD, Marmorstein R, Berger SL (2000) Phosphorylation of serine 10 in histone H3 is functionally linked in vitro and in vivo to Gcn5-mediated acetylation at lysine 14. *Mol Cell* 5: 917−926

Mahajan K, Fang B, Koomen JM, Mahajan NP (2012) H2B Tyr37 phosphorylation suppresses expression of replication-dependent core histone genes. *Nat Struct Mol Biol* 19: 930−937

Mahajan K, Malla P, Lawrence HR, Chen Z, Kumar-Sinha C, Malik R, Shukla S, Kim J, Coppola D, Lawrence NJ et al (2017) ACK1/TNK2 regulates histone H4 Tyr88-phosphorylation and AR gene expression in castration-resistant prostate cancer. *Cancer Cell* 31: 790−803

Marshall NF, Peng J, Xie Z, Price DH (1996) Control of RNA polymerase II elongation potential by a novel carboxyl-terminal domain kinase. *J Biol Chem* 271: 27176−27183

Meas R, Mao P (2015) Histone ubiquitylation and its roles in transcription and DNA damage response. *DNA Repair (Amst)* 36: 36−42

Rossetto D, Avvakumov N, Cote J (2012) Histone phosphorylation: a chromatin modification involved in diverse nuclear events. *Epigenetics* 7: 1098−1108

Sakai K, Tanaka Y, Asahi M, Shimomura R, Taniguchi T, Hashimoto E, Yamamura H (1991) Identification of the phosphorylation sites of H2B histone by a catalytic fragment of p72syk from porcine spleen. *FEBS Lett* 294: 104−108

Shechter D, Dormann HL, Allis CD, Hake SB (2007) Extraction, purification and analysis of histones. *Nat Protoc* 2: 1445−1457

Shilatifard A (2006) Chromatin modifications by methylation and ubiquitination: Implications in the regulation of gene expression. *Annu Rev Biochem* 75: 243−269

Suganuma T, Workman JL (2008) Crosstalk among histone modifications. *Cell* 135: 604−607

Svejstrup JQ (2004) The RNA polymerase II transcription cycle: cycling through chromatin. *Biochim Biophys Acta* 1677: 64−73

Tachiwana H, Osakabe A, Kimura H, Kurumizaka H (2008) Nucleosome formation with the testis-specific histone H3 variant, H3t, by human nucleosome assembly proteins in vitro. *Nucleic Acids Res* 36: 2208−2218

Takahashi A, Tsutsumi R, Kikuchi I, Obuse C, Saito Y, Seidi A, Karisch R, Fernandez M, Cho T, Ohnishi N et al (2011) SHP2 tyrosine phosphatase converts parafibromin/Cdc73 from a tumor suppressor to an oncogenic driver. *Mol Cell* 43: 45−56

Van Oss SB, Cucinotta CE, Arndt KM (2017) Emerging insights into the roles of the Paf1 complex in gene regulation. *Trends Biochem Sci* 42: 788−798

Van Zant G, Shultz L (1989) Hematologic abnormalities of the immunodeficient mouse mutant, viable motheaten (mev). *Exp Hematol* 17: 81−87

Varone A, Spano D, Corda D (2020) Shp1 in solid cancers and their therapy. *Front Oncol* 10: 935

Wei Y, Mizzen CA, Cook RG, Gorovsky MA, Allis CD (1998) Phosphorylation of histone H3 at serine 10 is correlated with chromosome condensation during mitosis and meiosis in Tetrahymena. *Proc Natl Acad Sci USA* 95: 7480−7484

Yang W, Tabrizi M, Yi T (2002) A bipartite NLS at the SHP-1 C-terminus mediates cytokine-induced SHP-1 nuclear localization in cell growth control. *Blood Cells Mol Dis* 28: 63−74

Yao X, Tang Z, Fu X, Yin J, Liang Y, Li C, Li H, Tian Q, Roeder RG, Wang G (2015) The mediator subunit MED23 couples H2B mono-ubiquitination to transcriptional control and cell fate determination. *EMBO J* 34: 2885−2902

Yeo M, Lin PS, Dahmus ME, Gill GN (2003) A novel RNA polymerase II C-terminal domain phosphatase that preferentially dephosphorylates serine 5. *J Biol Chem* 278: 26078−26085

Yip SS, Crew AJ, Gee JM, Hui R, Blamey RW, Robertson JF, Nicholson RI, Sutherland RL, Daly RJ (2000) Up-regulation of the protein tyrosine phosphatase SHP-1 in human breast cancer and correlation with GRB2 expression. *Int J Cancer* 88: 363−368

Zhang Q, Raghunath PN, Vonderheid E, Odum N, Wasik MA (2000) Lack of phosphotyrosine phosphatase SHP-1 expression in malignant T-cell lymphoma cells results from methylation of the SHP-1 promoter. *Am J Pathol* 157: 1137−1146

Zhang D, Tang Z, Huang H, Zhou G, Cui C, Weng Y, Liu W, Kim S, Lee S, Perez-Neut M *et al* (2019) Metabolic regulation of gene expression by histone lactylation. *Nature* 574: 575–580

Zhu B, Zheng Y, Pham AD, Mandal SS, Erdjument-Bromage H, Tempst P, Reinberg D (2005) Monoubiquitination of human histone H2B: The factors involved and their roles in HOX gene regulation. *Mol Cell* 20: 601–611